Modeling and Analysis of Limit Cycles in Buck Converters under PI Control

Mahnaz Yektaii

December 2004

Your file Votre référence
ISBN: 0-494-10680-8
Our file Notre référence
ISBN: 0-494-10680-8

To my family,

for their unconditional, everlasting love.

Abstract

A zero order hold equivalent discrete-time model of the buck converter for computing its large signal frequency-response is developed and experimentally verified. It is shown that with a dc bias and a sinusoidal variation of the input duty cycle, the frequency-response of the output voltage from the converter shifts from underdamped behaviour to damped behaviour with increasing amplitude of the input sinusoid. It is observed that with a given dc input bias and a given input amplitude beyond the range of the state-space averaged small signal model, the converter behaviour varies from exclusively continuous inductor current mode at low frequencies to behaviour with continuous and discontinuous inductor current modes at high frequencies. The use of this sinusoidal input large signal frequency-response in predicting limit cycles induced by feedback of output voltage using proportional and integral controllers for such converters is studied. Experimental results confirming the use of this large signal frequency-response are presented. Also the use of large signal model in predicting the steady-state behaviour is studied.

Acknowledgment

Dr. K. Natarjan's extreme help and guidance made this work possible. I sincerely appreciate his patience with me and admire his support and understanding.

Contents

List of Figures

Chapter 1

Introduction

1.1 The overview of literature

Linear time-invariant small signal state-space averaged models [1], [5] of PWM converters in exclusive operation modes such as continuous inductor current or discontinuous inductor current is standard in the literature for stability analysis of controller designs. Extensions of the method to include more Fourier components in the state-space description and thus to include a larger signal range along the lines of multi-frequency averaging [8], [9], [10] for fast computer simulation of such converters make similar assumptions. However, when limit cycles arise in such converters under analog feedback, the converter behaviour is governed by the presence of both continuous and discontinuous current modes. Analysis assuming that the converter stays in one exclusive mode of behaviour is not useful. Since the time at which the converter enters discontinuous mode is governed by internal states of the converter, recent work in modeling has been aimed at developing small signal models of discontinuous mode of operation of such converters [11], [12]. For limit cycle predictions, however large signal frequency-response as a function of the amplitude of the sinusoidal input (duty cycle) signal along with a dc bias is needed [4], [13]. In this thesis, such a large signal frequency-response is derived for the buck converter using a ZOH equivalent discrete-time model and experimentally confirmed. ZOH modeling of state-space descriptions is very commonly used in digital control [14], but has been used only sporadically in power electronic circuits [15], [16], [17]. This method however has the potential of developing frequency-response characteristics in all operating modes of the converter. It is this latter potential of the technique that is exploited in this thesis.

1.2 Thesis outline

The organization of the thesis is as follows. Chapter 1 continues with an introduction on the basic concept of the buck converter. In Chapter 2 different models of the buck converter are introduced. The models include, state-space averaged small signal model, large signal model, which is developed in this thesis, linearized discrete model, which is also

developed in this thesis and Fourier series model. Unlike other introduced models the large signal model, which is a ZOH discrete-time model of the buck converter, is developed for both continuous and discontinuous modes of operation. Thereafter this is used to predict and experimentally verify the limit cycle behaviour for the buck converter operated with analog PI controls. In Chapter 3 the behavior of the models of Chapter 2 are studied in terms of frequency-response and compared. The large signal continuous-time frequency-response of the converter derived from the discrete-time model is experimentally verified. The continuous-time frequency-response is needed since controllers for such converters are implemented in the analog domain. In Chapter 4, the large signal model is used to predict the limit cycles and output voltage ripple of the buck converter. The large signal frequency-response is used to predict the limit cycle frequency and amplitude when the converter is operated with analog PI control. Experimental results of such behaviour are presented and compared to predicted results. Chapter 5 studies the buck converter when load current, input voltage or the inductance value varies and suggests the future work based on that and concludes the thesis.

1.3 DC-DC switch-mode converters

dc-dc converters are used to convert an unregulated dc voltage into a regulated dc voltage at a desired voltage level. Switch-mode converters utilize a switch to do the conversion and compared to linear power supplies, they are more flexible and provide higher efficiency.

1.4 Step-down (buck) converters

A buck converter produces an average output voltage V_o lower than the dc input voltage V_d. Figure 1.1 shows the basic circuit of a buck converter and its output voltage waveform. The average value V_o of the output voltage v_o depends on the switch on and off durations (t_{on} and t_{off}). In other words, the average output voltage can be controlled by varying duty ratio of switch d as shown in (1.1).

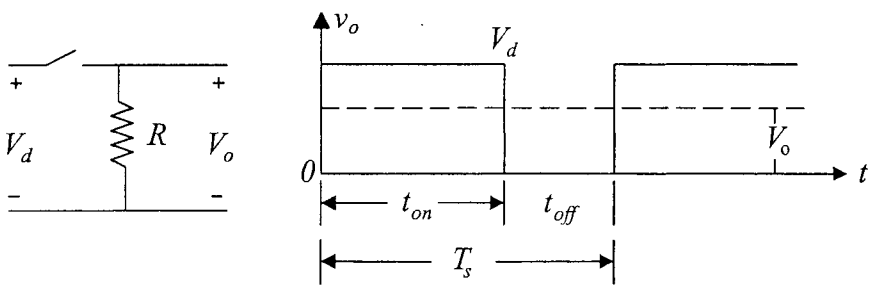

Figure 1.1: Basic circuit of a buck converter and its output waveform

$$V_o = \frac{t_{on}}{T_s} V_d = dV_d \tag{1.1}$$

Figure 1.2 shows the practical buck converter circuit. An ideal low-pass filter is added to diminish the output voltage fluctuations, and a diode to allow the current flow while the switch is off. When the switch is on, the diode becomes reverse biased and the input provides energy to the load. When the switch is off, the inductor current flows through the diode transferring some of its stored energy to the load. This ensures a relatively low ripple voltage on the load.

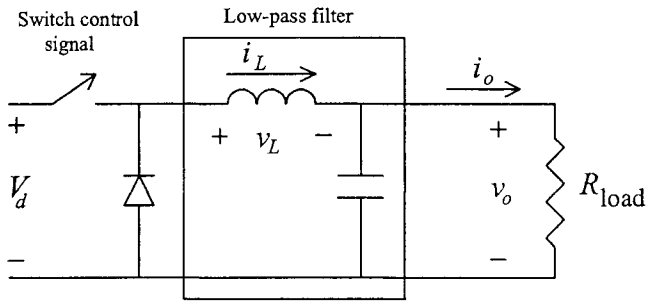

Figure 1.2: Buck converter

1.5 Control of buck converter

The control objective in a buck converter is to maintain V_o at a desired level, in spite of the fluctuations in V_d and load. Pulse-width modulation (PWM) switching is one of the methods for controlling V_o that employs switching at a constant frequency and adjusting *on* duration of switch in order to ensure $V_o = V_{ref}$.

As shown in Figure 1.3 duty cycle of switch control signal is generated by comparing output of PI controller with a repetitive saw-tooth waveform. The frequency f_s and the amplitude $\hat{V}_{st}$ of the saw-tooth waveform is constant. It can be shown that duty cycle of switch control signal d varies proportionally with output of controller $v_{control}$

$$d = \frac{v_{control}}{\hat{V}_{st}}. \tag{1.2}$$

1.6 Modes of operation

There are two modes of operation based on the value of inductor current. When the switch is on, the inductor current i_L increases, and during t_{off}, i_L decreases as it flows through the diode. If the inductor current flows continuously over a switching period, the converter is said to be working in *continuous-conduction mode* of operation (Figure 1.4). And if it gets to zero for an interval in the t_{off} period, it is working in *discontinuous-conduction mode* (Figure 1.5).

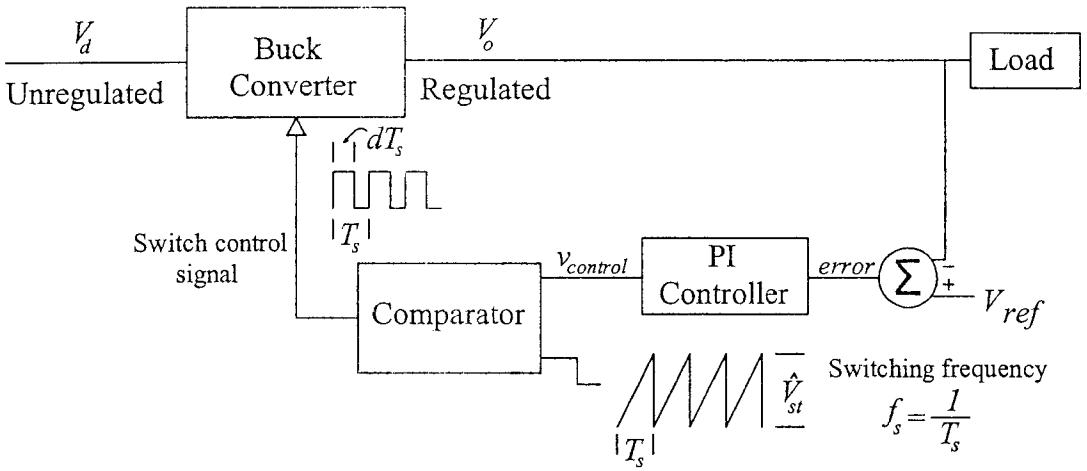

Figure 1.3: Controller circuit of a buck converter

At the boundary between continuous and discontinuous mode, the inductor current goes to zero exactly at the end of t_{off}. At this boundary, in the buck converter of Figure 1.2 with ideal elements, the average inductor current is,

$$I_{LB} = \frac{dT_s}{2L}(V_d - V_o). \tag{1.3}$$

Maximum value of I_{LB} occurs at $d = 0.5$, given by, $I_{LB,max} = \frac{T_s V_d}{8L}$.

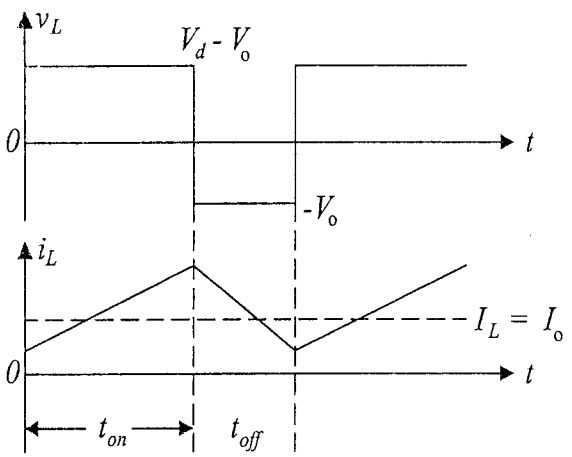

Figure 1.4: Inductor voltage and current in continuous-conduction mode

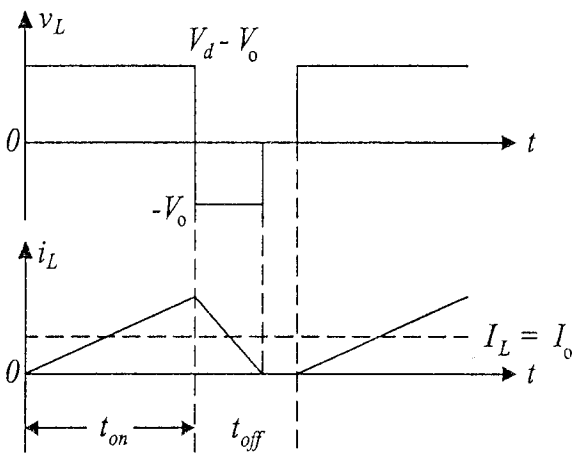

Figure 1.5: Inductor voltage and current in discontinuous-conduction mode

Therefore, for a given set of ideal parameters, if $I_L > I_{LB}$, the converter is in continuous-conduction mode else it is in discontinuous-conduction mode.

1.7 Output voltage ripple

Assuming that all of the ripple component in i_L flows through the capacitor and its average component flows through the load resistor, the ripple in the output voltage for a continuous-conduction mode of operation with ideal low pass filter of Figure 1.2 can be expressed as [1],

$$\frac{\Delta V_o}{V_o} = \frac{\pi^2}{2}\,(1-d)\,(\frac{f_c}{f_s})^2. \tag{1.4}$$

Where switching frequency $f_s = \frac{1}{T_s}$ and cut-off frequency of the low-pass filter is,

$$f_c = \frac{1}{2\pi\sqrt{LC}}. \tag{1.5}$$

Equation (1.4) shows that ripple can be minimized, if cut-off frequency is selected much lower than switching frequency. It also shows that ripple is independent of the value of load but depends on L and C, assuming no losses in circuit.

Chapter 2

Models of the buck converter

In this chapter some approaches to modeling of a buck converter with non-ideal filter are introduced. In Section 2.1, the basic equations of a buck converter are derived. The models discussed in following sections are based on these equations.

2.1 Differential equations of a buck converter

Figure 2.1 shows the basic topology of a buck converter. The parasitic elements are included as r_L for the inductor resistance and r_C for the equivalent series resistance (ESR) of the capacitor. The diode and switch are considered to be ideal and it is assumed that in continuous-conduction mode of operation, when the switch is on, the diode is off and when the switch is off, the diode is on.

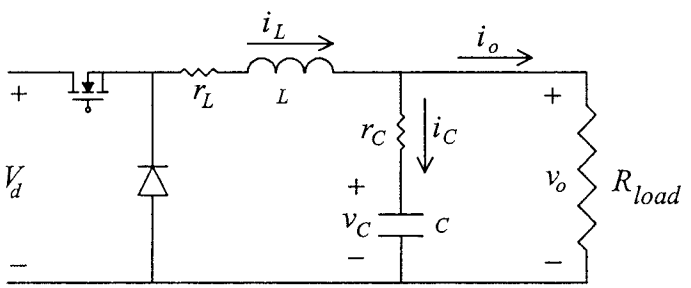

Figure 2.1: Buck converter circuit

By considering that $i_L > 0$ and the switch is on and the diode is off, the following equations can be derived,

$$-V_d + r_L i_L(t) + L\frac{di_L(t)}{dt} + v_o(t) = 0$$

$$-v_C(t) - C\frac{dv_C(t)}{dt}\, r_C + v_o(t) = 0$$

$$v_o(t) = R_{load}\,(i_L(t) - C\frac{dv_C(t)}{dt})$$

where i_L is the inductor current, v_C is the capacitor voltage and v_o is the voltage across the load. When the switch is off and the diode is on, the set of equations in (2.1) are applicable, but with $V_d = 0$. In matrix form, the differential equations can be written as,

$$\frac{d}{dt}\begin{bmatrix} i_L(t) \\ v_C(t) \end{bmatrix} = \begin{bmatrix} -\frac{R_{load}r_C + R_{load}r_L + r_C r_L}{L(R_{load}+r_C)} & -\frac{R_{load}}{L(R_{load}+r_C)} \\ \frac{R_{load}}{C(R_{load}+r_C)} & -\frac{1}{C(R_{load}+r_C)} \end{bmatrix}\begin{bmatrix} i_L(t) \\ v_C(t) \end{bmatrix} + \begin{bmatrix} \frac{1}{L} \\ 0 \end{bmatrix} V_d s \quad (2.1)$$

$$v_o(t) = \begin{bmatrix} \frac{R_{load}r_C}{R_{load}+r_C} & \frac{R_{load}}{R_{load}+r_C} \end{bmatrix}\begin{bmatrix} i_L(t) \\ v_C(t) \end{bmatrix}$$

where s is 1 if the switch is on (and the diode is off) and 0 if the switch is off (and the diode is on).

During discontinuous-conduction mode of operation, for $i_L = 0$, both switch and diode are off and Equation (2.1) reduces to,

$$\frac{d}{dt}\begin{bmatrix} i_L(t) \\ v_C(t) \end{bmatrix} = \begin{bmatrix} 0 & 0 \\ 0 & -\frac{1}{C(R_{load}+r_C)} \end{bmatrix}\begin{bmatrix} i_L(t) \\ v_C(t) \end{bmatrix} \quad (2.2)$$

$$v_o(t) = \begin{bmatrix} 0 & \frac{R_{load}}{R_{load}+r_C} \end{bmatrix}\begin{bmatrix} i_L(t) \\ v_C(t) \end{bmatrix}.$$

Considering the state-variable vector x consisting of the inductor current i_L and capacitor voltage v_C respectively, and

$$A = \begin{bmatrix} -\frac{R_{load}r_C + R_{load}r_L + r_C r_L}{L(R_{load}+r_C)} & -\frac{R_{load}}{L(R_{load}+r_C)} \\ \frac{R_{load}}{C(R_{load}+r_C)} & -\frac{1}{C(R_{load}+r_C)} \end{bmatrix},\ B = \begin{bmatrix} \frac{1}{L} \\ 0 \end{bmatrix},\ C = \begin{bmatrix} \frac{R_{load}r_C}{R_{load}+r_C} & \frac{R_{load}}{R_{load}+r_C} \end{bmatrix},$$

for $i_L > 0$, or

$$A = \begin{bmatrix} 0 & 0 \\ 0 & -\frac{1}{C(R_{load}+r_C)} \end{bmatrix},\ B = \begin{bmatrix} 0 \\ 0 \end{bmatrix},\ C = \begin{bmatrix} 0 & \frac{R_{load}}{R_{load}+r_C} \end{bmatrix}$$

for $i_L = 0$, the state space representation of the system can be written as,

$$\dot{x} = Ax + BV_d\, s \quad (2.3)$$
$$v_o = Cx.$$

The assumptions and equations given in this section are the basis of the models discussed in the following sections of this chapter.

2.2 Small signal model using state-space averaging

[1] and [5] have introduced a state-space averaging technique that results in a linear model of the buck converter for input duty cycle variations around a steady-state operating point.

There are usually two major assumptions made for deriving this small signal model which are as follows,

1) Variations around the steady-state operating point are very small.
2) The buck converter is operating in continuous-conduction mode.

2.2.1 State-space description

Since the converter is considered to be working in continuous-conduction mode there are two circuit states, one with switch on and diode off and the other with switch off and diode on. The state space representation of the system in (2.3) for when the switch is on ($s = 1$) can be written as,

$$\begin{aligned} \dot{x} &= Ax + BV_d \qquad \text{during switch on: } d\,T_s \\ v_o &= Cx. \end{aligned}$$

These state equations with the switch off ($s = 0$) will be,

$$\begin{aligned} \dot{x} &= Ax \qquad \text{during switch off: } (1-d)\,T_s \\ v_o &= Cx. \end{aligned}$$

The equations for each state are time weighted and averaged over a switching period T_s resulting in the following equations,

$$\begin{aligned} \dot{x} &= Ax + BdV_d \\ v_o &= Cx \end{aligned} \tag{2.4}$$

where d is the duty ratio of the switch control signal.

2.2.2 Separation into ac and dc components

Small ac perturbations $\tilde{x}$, $\tilde{v}_o$ and $\tilde{d}$ are introduced in (2.4) by splitting variables x, v_o and d into ac and dc components,

$$x = X + \tilde{x} \qquad v_o = V_o + \tilde{v}_o \qquad d = D + \tilde{d} \tag{2.5}$$

where X,V_o and D are dc steady-state quantities.

By substituting x, v_o and d from (2.5) in (2.4) and considering that in steady-state $\dot{X} = AX + BDV_d = 0$, (2.4) can be simplified as,

$$\begin{aligned} \dot{\tilde{x}} &= A\tilde{x} + B\tilde{d}V_d \\ \tilde{v}_o &= C\tilde{x}. \end{aligned} \tag{2.6}$$

2.2.3 Pulse-width modulator

From (1.2) it can be shown that,

$$\tilde{d} = \frac{\tilde{v}_{control}}{\hat{V}_{st}}. \tag{2.7}$$

By substituting (2.7), Equation (2.6) can be written as,

$$\begin{aligned} \dot{\tilde{x}} &= A\tilde{x} + B\,\frac{V_d}{\hat{V}_{st}}\,\tilde{v}_{control} \\ \tilde{v}_o &= C\tilde{x}. \end{aligned} \tag{2.8}$$

Equation (2.8) gives the small signal transfer function $\frac{\tilde{v}_o(s)}{\tilde{v}_{control}(s)}$ where $\tilde{v}_o$ and $\tilde{v}_{control}$ are small perturbations in the output voltage V_o and control (or input) voltage $V_{control}$ respectively. With some simplifications,

$$\frac{\tilde{v}_o(s)}{\tilde{v}_{control}(s)} = \frac{V_d}{\hat{V}_{st}}\,\frac{1 + sr_CC}{LC\,(s^2 + s\,(\frac{1}{RC} + \frac{r_C+r_L}{L}) + \frac{1}{LC})}. \tag{2.9}$$

The state space representation of Equation (2.8) or its simplified transfer function in (2.9) are used for the analysis of small signal model.

A similar averaging technique can be carried out for a converter working in discontinuous-conduction mode [6].

2.3 Large signal model

A new large signal model developed in this thesis is introduced here. The small signal model assumes that perturbations are very small and the converter always works in continuous-conduction mode. However for large perturbations in duty cycle, the converter will not operate in continuous-conduction mode only but will exhibit continuous and discontinuous modes of operation. So the large signal model is developed based on both modes of operation and can predict the large signal behavior of the converter.

2.3.1 Discrete time state space representation

In the development of the large signal model, it is assumed that the duty cycle d ($0 \leq d \leq 1$) of the switch can be affected only once in every switching period T_s. Since in practice the switching periods are being pushed to smaller values, this assumption is reasonable to make for modeling purposes. It is also assumed that the switching frequency $f_s = \frac{1}{T_s}$ is much greater than the resonant frequency f_c which is needed almost always for voltage ripple reduction (1.4).

At intervals of switching period the state space representation in (2.3) can be discretized as,

$$\begin{aligned} x_{(k+d_k)T_s} &= F_1 x_{kT_s} + G_1 V_d \qquad \text{during switch on: } d_k\ T_s & (2.10)\\ x_{(k+1)T_s} &= F_3 F_2 x_{(k+d_k)T_s} \qquad \text{during switch off: } (1-d_k)\ T_s & (2.11)\\ v_{o_{kT_s}} &= C x_{kT_s}. \end{aligned}$$

Where F_1, F_2, F_3 and G_1 are obtained as per,

$$\begin{aligned} F_1 &= e^{Ad_kT_s} \quad G_1 = (F_1 - I)A^{-1}B & (2.12)\\ F_2 &= e^{A(1-d_k)T_s} \text{ if } \phi_k \geq (1-d_k)T_s & (2.13)\\ F_2 &= e^{A\phi_k} \text{ if } \phi_k < (1-d_k)T_s & (2.14)\\ F_3 &= I \text{ if } \phi_k \geq (1-d_k)T_s & (2.15)\\ F_3 &= \begin{bmatrix} 1 & 0 \\ 0 & e^{a_{22}((1-d_k)T_s - \phi_k)} \end{bmatrix} \text{ if } \phi_k < (1-d_k)T_s & (2.16) \end{aligned}$$

and ϕ_k is the time duration taken by inductor current i_L to become zero after the switch is turned off in the k$^{\text{th}}$ switching cycle and d_k is the duty cycle in the k$^{\text{th}}$ switching cycle.

The terms, ϕ_k, F_2 and F_3 are explained and derived in the next two sections.

2.3.2 Calculation of ϕ

When switch is off, $s = 0$ and the state space representation in (2.3) can be written as,

$$\dot{x} = Ax$$

which implies,

$$x = e^{At}x_0 = Pe^{\Lambda t}P^{-1}x_0 \tag{2.17}$$

where Λ and P are diagonal matrix and eigenvector matrix of matrix A respectively and x_0 is the initial value of the state vector when switch is turned off.
Equation (2.17) can be written as,

$$\begin{bmatrix} i_L(t) \\ v_C(t) \end{bmatrix} = \begin{bmatrix} \frac{p_{22}}{p_{11}p_{22}-p_{21}p_{12}} & \frac{-p_{12}}{p_{11}p_{22}-p_{21}p_{12}} \\ \frac{-p_{21}}{p_{11}p_{22}-p_{21}p_{12}} & \frac{p_{11}}{p_{11}p_{22}-p_{21}p_{12}} \end{bmatrix} \begin{bmatrix} e^{\lambda_1 t} & 0 \\ 0 & e^{\lambda_2 t} \end{bmatrix} \begin{bmatrix} p_{11} & p_{12} \\ p_{21} & p_{22} \end{bmatrix} \begin{bmatrix} i_{L(k+d)T_s} \\ v_{C(k+d)T_s} \end{bmatrix} \tag{2.18}$$

where p_{ij} denote the elements of the P^{-1} matrix, and λ_1, λ_2 are eigenvalues of matrix A. Considering $i_L = 0$ and solving (2.18) for time t, ϕ_k can be obtained as,

$$\phi_k = \frac{\ln\left(\frac{\left(p_{21}i_{L_{(k+d)T_s}} + p_{22}v_{C_{(k+d)T_s}}\right)p_{12}}{\left(p_{11}i_{L_{(k+d)T_s}} + p_{12}v_{C_{(k+d)T_s}}\right)p_{22}}\right)}{\lambda_1 - \lambda_2} \tag{2.19}$$

where the inductor current $i_{L_{(k+d)T_s}}$ and capacitor voltages $v_{C_{(k+d)T_s}}$ are the elements of x_0 in (2.17) and can be obtained from Equation (2.10).

It can be seen that the value of ϕ_k is logarithmically dependent on previous state variables. So the large signal model is a nonlinear model of the buck converter where the nonlinearity appears in ϕ_k, should the discontinuous-conduction mode be present in the operation of the converter.

2.3.3 Calculations of F_2 and F_3

Two states are possible while switch is off, one when inductor current flows ($i_L > 0$, diode is on) upto the end of the switching period and one when inductor current goes to zero before the end of switching period ($i_L = 0$, diode is off).

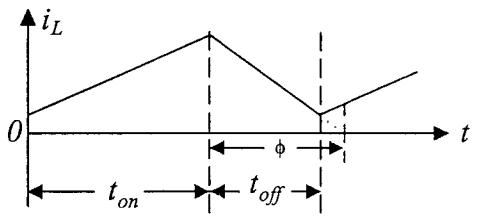

Figure 2.2: Inductor current and ϕ in continuous-conduction mode

As shown in Figure 2.2, if $\phi_k \geq t_{off}$, that means the inductor current flows during t_{off} and converter is in continuous-conduction mode. In this case F_2 and F_3 in (2.11) are obtained as,

$$\begin{aligned} F_2 &= e^{A(1-d)T_s} \\ F_3 &= I. \end{aligned}$$

Figure 2.3 shows the situation for $\phi_k < t_{off}$, when inductor current is zero for some duration of t_{off} and so converter is working in discontinuous-conduction mode.

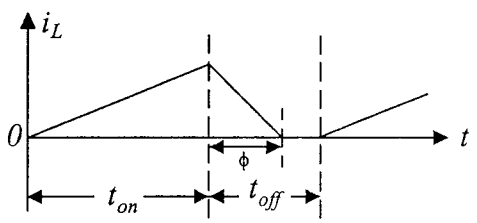

Figure 2.3: Inductor current and ϕ in discontinuous-conduction mode

In this case, during time ϕ_k the equations for $i_L > 0$ are applied to converter and F_2 in (2.11) is calculated as,

$$F_2 = e^{A\phi_k}.$$

And for the rest of the switch off time *i.e.* $(1-d)T_s - \phi_k$ the equations for $i_L = 0$ are applied and F_3 in (2.11) can be calculated as,

$$F_3 = e^{A((1-d)T_s - \phi_k)}$$

with $A = \begin{bmatrix} 0 & 0 \\ 0 & -\frac{1}{C(R_{load}+r_C)} \end{bmatrix}$, which gives,

$$F_3 = \begin{bmatrix} 1 & 0 \\ 0 & e^{a_{22}((1-d)T_s - \phi_k)} \end{bmatrix}$$

where $a_{22} = -\frac{1}{C(R_{load}+r_C)}$.

2.4 Simulation model (using C-code)

A straight forward modeling technique for the buck converters is to solve the differential equations of the buck converter (section 2.1) and controller in small time steps in order to obtain the instantaneous values of capacitor voltage, inductor current and any other desired parameter in the circuit.

The software to accomplish this, is implemented using C programming language in this thesis. Referring to Figure 1.3, at each time step, the simulation program does the following,

- Calculates control signal $v_{control}$ using *error* at input of a PI controller.
- Determines the status of the switch based on comparison between the control signal $v_{control}$ and a sawtooth waveform generated in the code.
- Updates values of inductor current i_L and capacitor voltage v_o by solving differential equations of the buck converter (section 2.1). The differential equations are solved using the fourth-order Runge-Kutta method.
- Calculates the *error* in output voltage by subtracting instantaneous voltage v_o from V_{ref}.

The above mentioned steps are considered for a buck converter in closed-loop situation. In order to study the buck converter behaviour without the controller, for instance to find the frequency-response of the buck converter, the desired values can be given to the input signal $v_{control}$ directly, with the controller portion of the code turned off.

The code time step is considered equal to 0.02μs which is equivalent to more than 1600 samples per switching period for a switching frequency of $f_s = 30$kHz. The software is executed usually for sufficient time to achieve the steady-state of the output voltage and the data obtained from this code is processed using MATLAB. The step size chosen is a compromise between overall time of simulation and accuracy with an emphasis on accuracy.

The results of the C-code simulation method, as shown in the next chapter, are very similar to experimental results but due to the complexity of calculations, C-code simulation takes a long processing time.

2.5 Linearized discrete model

This model is derived from the large signal model of Section 2.3 with the assumption that the buck converter operates only in continuous-conduction mode. Therefore two circuit states exist, one when switch is on (and diode is off) and the other when the switch is off (and diode is on). With a sampling time equal to switching period T_s, Equations (2.10) and (2.11) are now,

$$x_{(k+d_k)T_s} = F_1 x_{kT_s} + G_1 V_d \qquad \text{during switch on: } d_k T_s \tag{2.20}$$

$$x_{(k+1)T_s} = F_2 x_{(k+d_k)T_s} \qquad \text{during switch off: } (1-d_k)T_s \tag{2.21}$$

where $F_1 = e^{Ad_kT_s}$, $G_1 = (F_1 - I)A^{-1}B$ and $F_2 = e^{A(1-d_k)T_s}$.
From (2.20) and (2.21) the discrete representation of the buck converter operating in continuous-conduction mode at intervals of switching frequency is obtained as,

$$\begin{cases} x_{(k+1)T_s} = F x_{kT_s} + F_2 G_1 V_d \\ v_{o_{kT_s}} = C x_{kT_s} \end{cases} \tag{2.22}$$

where $F = F_2 F_1 = e^{AT_s}$.
It can be seen that F does not depend on duty cycle d_k, but since $F_2 G_1$ is exponentially dependent on input d_k, the system in equation (2.22) through $F_2 G_1$ is nonlinear in d_k.

2.5.1 Nonlinear discrete model

The describing function analysis used to predict self-sustained oscillations (limit cycles) of non-linear time-invariant systems [7], is used further to split the system into non-linear and linear parts. The nonlinearities are then replaced with signal-dependent linear gains. This provides a way to take advantage of linear system approaches to understand the behaviour of the nonlinear system. Based on this idea, the closed loop non-linear system of (2.22), can be brought into the form indicated in Figure 2.4. The figure shows the system, separated into non-linear and linear parts.

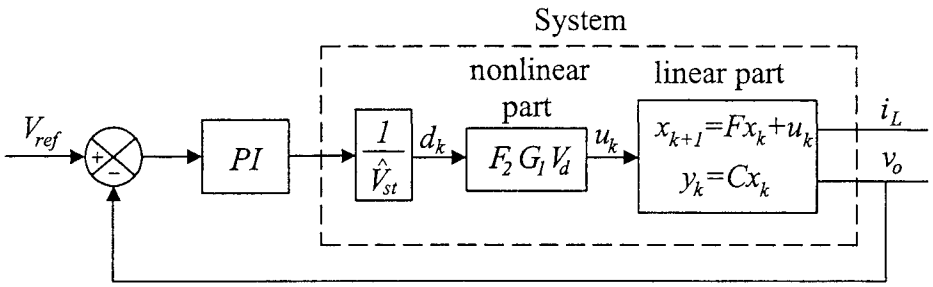

Figure 2.4: Nonlinear system of (2.22) in closed loop form

The vector u_k is a 2×1 vector with components $u_{11}(d_k)$ and $u_{21}(d_k)$. A graphical variation of u_{11} and u_{21} as a function of d_k is obtained in Figures 2.5 and 2.6 (for converter Buck2 in appendix A).

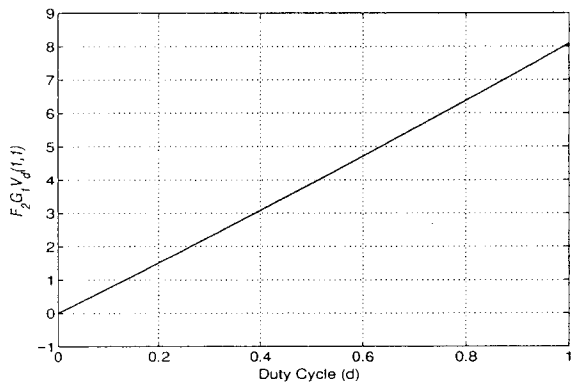

Figure 2.5: u_{11}

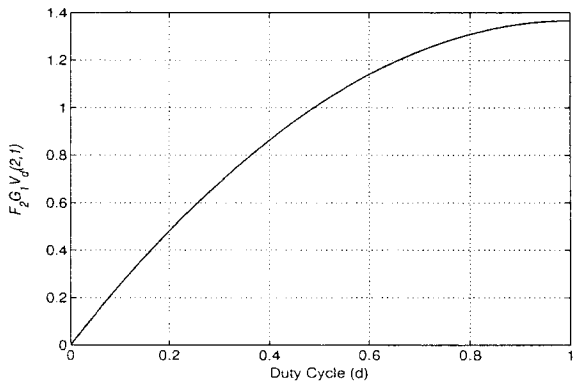

Figure 2.6: u_{21}

Curve-fitting is used to obtain the following equations.

$$u_{11}(d_k) = \begin{cases} -0.1051 & \text{for} \quad d_k < 0 \\ 8.0964 d_k - 0.1051 & \text{for} \quad 0 \leq d_k \leq 1 \\ 7.9913 & \text{for} \quad d_k > 1 \end{cases} \tag{2.23}$$

$$u_{21}(d_k) = \begin{cases} -0.0042 & \text{for} \quad d_k < 0 \\ -1.3278 {d_k}^2 + 2.7017 d_k - 0.0042 & \text{for} \quad 0 \leq d_k \leq 1 \\ 1.3698 & \text{for} \quad d_k > 1 \end{cases} \tag{2.24}$$

When a buck converter is in limit cycles around an operating point, the input duty cycle d and the output voltage v_o have a dc value plus a sinusoidal signal due to oscillation. So, the describing functions for buck converter should be obtained with the input signal considered as a sinusoid plus a dc bias.

By considering the equations given in (2.23,2.24) as the nonlinear part of the buck converter and $B + Asin(\omega t)$ as the input to the nonlinearity, describing functions N_0 and N_1 are obtained as per [7].

These describing functions were then used in a closed loop situation to predict the limit cycle amplitude and frequency. But the equations could not be solved for a rational value of oscillation frequency and amplitude of oscillation observed for choice of K_p and K_i gains. So, it was concluded that this approach is not capable of predicting limit cycles. However this model brings out the nonlinearity in the buck converter clearly and can be used to develop a small signal linearized model.

In the next chapter, we will see that, the primary assumption of buck converter working in continuous-conduction mode, does not hold when converter goes to oscillations and that is why the describing function equations obtained based on this assumption cannot be solved for limit cycles.

2.5.2 Linearization

It can be seen that the graph of Figure 2.5, which contributes to coupling the duty cycle d_k to the inductor current, is linear and the graph of Figure 2.6, which contributes to coupling duty cycle d_k to capacitor voltage, is nonlinear.

As, Figure 2.7 shows, the nonlinear graph can be linearized. The duty cycle at which the linearization is done is chosen as $d = 0.7177$ for Buck2 with properties given in Appendix A as this duty cycle is the operating point duty cycle of the buck converter.

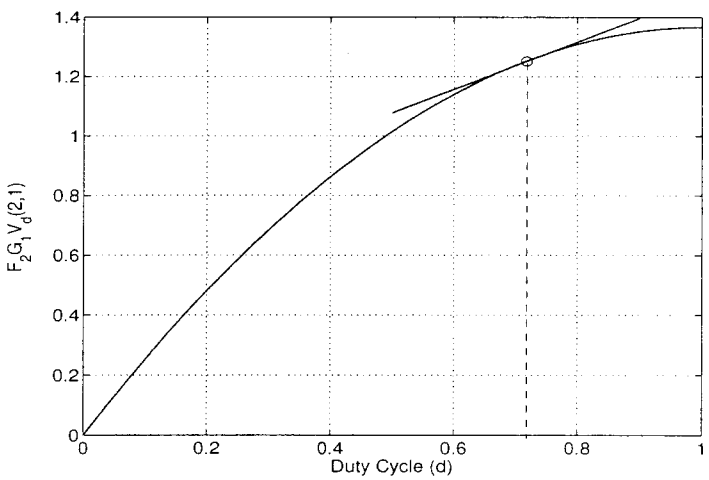

Figure 2.7: Linearization at the operating point ($d = 0.7177$)

The linearized equation or the tangent line equation can be expressed as,

$$u_{21}(d) = 0.7957d + 0.6798. \tag{2.25}$$

By substituting the slopes from equations (2.23) and (2.25) in the system shown in Figure 2.4, a linear transfer function for the buck converter can be obtained. It is obvious that, this linearized discrete model is valid only for small variation around the operating point.

Assuming that the buck converter is working around duty cycle operating point of $D = 0$, the linearized equation is,

$$u_{21}(d) = 2.7017d - 0.0042$$

and assuming that it is working around duty cycle operating point of $D = 1$, the linearized equation is,

$$u_{21}(d) = 0.0462d + 1.3236.$$

It can be seen that the linearized equations depend on the operating point of the buck converter and a large variation of slope is evident.

2.5.3 Analytic linearization

Considering $F_1 = e^{Ad_kT_s}$, $G_1 = (F_1 - I)A^{-1}B$ and $F_2 = e^{A(1-d_k)T_s}$, Equation 2.22, can be brought to the following form,

$$x_{(k+1)T_s} = e^{AT_s}x_{kT_s} + (e^{AT_s} - e^{A(1-d_k)T_s})A^{-1}BV_d. \tag{2.26}$$

Small perturbations $\delta x_{(k+1)T_s}$, δx_{kT_s} and δd_k are introduced in (2.26) as follows,

$$x_{(k+1)T_s} + \delta x_{(k+1)T_s} = e^{AT_s}(x_{kT_s} + \delta x_{kT_s}) + (e^{AT_s} - e^{A(1-d_k-\delta d_k)T_s})A^{-1}BV_d$$

or,

$$x_{(k+1)T_s} + \delta x_{(k+1)T_s} = e^{AT_s}(x_{kT_s} + \delta x_{kT_s}) + (e^{AT_s} - e^{A(1-d_k)T_s}e^{-A\delta d_k T_s})A^{-1}BV_d.$$

If changes in d_k are small $e^{-A\delta d_k T_s}$ can be approximated as $I - A\delta d_k\ T_s$ to obtain,

$$x_{(k+1)T_s} + \delta x_{(k+1)T_s} = e^{AT_s}(x_{kT_s} + \delta x_{kT_s}) + (e^{AT_s} - e^{A(1-d_k)T_s}(I - A\delta d_k\ T_s))A^{-1}BV_d.$$

The above can be written as,

$$\begin{aligned} x_{(k+1)T_s} + \delta x_{(k+1)T_s} \quad = \quad & e^{AT_s}(x_{kT_s} + \delta x_{kT_s}) + (e^{AT_s} - e^{A(1-d_k)T_s})A^{-1}BV_d + \\ & e^{A(1-d_k)T_s}\delta d_k\ T_sBV_d. \end{aligned} \tag{2.27}$$

Considering (2.26), Equation (2.27) can be simplified as,

$$\delta x_{(k+1)T_s} = e^{AT_s}\delta x_{kT_s} + (e^{A(1-d_k)T_s}BV_d)T_s\ \delta d_k \tag{2.28}$$

which is the analytic form of the linearized discrete model.

The linearized method introduced in Section 2.5.2 or the equivalent analytic form of it in (2.28) is called the linearized discrete model and will be discussed further in the next chapter.

2.6 Fourier series model

An approach to modeling the dynamic behaviour of pulse width modulated (PWM) dc-dc converters is introduced in [8] and further investigated in [9]. The method is based on the Fourier series representation of inductor current and the capacitor voltage. The average of the signals are computed by taking into account the constants in the Fourier series and the ripple in signals are estimated by considering the harmonics of the fundamental frequency which is the same as switching period. It is mentioned that in order to increase the accuracy of the model, higher harmonics have to be included. Later on [10] expands the idea presented in [9] by including higher harmonics (more Fourier coefficients) in calculations. In this section the details of the model presented in [10] are applied to a buck converter and the results are studied.

2.6.1 Fourier series

Fourier series representation of a signal $x(\tau)$ on the interval $[t-T_s, t]$ is given as,

$$x(\tau) = \sum_{k=-\infty}^{\infty} \langle x \rangle_k(t) e^{jk\omega_s \tau}$$

where $\omega_s = \frac{2\pi}{T_s}$ and $\langle x \rangle_k(t)$ are the Fourier coefficients given by,

$$\langle x \rangle_k(t) = \frac{1}{T_s} \int_{t-T_s}^{t} x(\tau) e^{-jk\omega_s \tau} d\tau.$$

From [10] the time derivative of the k^{th} coefficient is computed to be,

$$\frac{d}{dt}\langle x \rangle_k(t) = -jk\omega_s \langle x \rangle_k(t) + \langle \frac{d}{dt} x \rangle_k(t) \tag{2.29}$$

which is the key property used in such Fourier series analysis.

2.6.2 Buck converter in open loop situation

The method assumes that converter is operating in continuous-conduction mode. The buck converter equations in (2.1) can be presented as follows,

$$\begin{aligned} \frac{d}{dt} i_L(t) &= -\frac{R_{load} r_C + R_{load} r_L + r_C r_L}{L(R_{load} + r_C)} i_L(t) - \frac{R_{load}}{L(R_{load} + r_C)} v_C(t) + \frac{1}{L} q(t) V_d \\ \frac{d}{dt} v_C(t) &= \frac{R_{load}}{C(R_{load} + r_C)} i_L(t) - \frac{1}{C(R_{load} + r_C)} v_C(t) \end{aligned} \tag{2.30}$$

where $q(t)$ is the switching function and for the open-loop situation it is described as follows,

$$q(t) = \begin{cases} 1, & \text{for} \quad 0 \le t < dT_s \\ 0, & \text{for} \quad dT_s \le t < T_s \end{cases}$$

assuming that duty ratio d is fixed with $0 \leq d \leq 1$ and T_s is the switching period.

By replacing the time-varying signals in (2.30) with their Fourier coefficients for all integer k, the following equations are obtained.

$$\begin{aligned}
\langle \frac{d}{dt} i_L \rangle_k &= -\frac{R_{load}r_C + R_{load}r_L + r_C r_L}{L(R_{load} + r_C)} \langle i_L \rangle_k - \frac{R_{load}}{L(R_{load} + r_C)} \langle v_C \rangle_k + \frac{1}{L} \langle q \rangle_k V_d \\
\langle \frac{d}{dt} v_C \rangle_k &= \frac{R_{load}}{C(R_{load} + r_C)} \langle i_L \rangle_k - \frac{1}{C(R_{load} + r_C)} \langle v_C \rangle_k
\end{aligned}$$

Using Fourier series property from (2.29) the above can be rewritten as,

$$\begin{aligned}
\frac{d}{dt} \langle i_L \rangle_k &= -jk\omega_s \langle i_L \rangle_k - \frac{R_{load}r_C + R_{load}r_L + r_C r_L}{L(R_{load} + r_C)} \langle i_L \rangle_k - \frac{R_{load}}{L(R_{load} + r_C)} \langle v_C \rangle_k + \frac{1}{L} \langle q \rangle_k V_d \\
\frac{d}{dt} \langle v_C \rangle_k &= -jk\omega_s \langle v_C \rangle_k + \frac{R_{load}}{C(R_{load} + r_C)} \langle i_L \rangle_k - \frac{1}{C(R_{load} + r_C)} \langle v_C \rangle_k. \qquad (2.31)
\end{aligned}$$

The above equations can be seen as a set of differential equations by which $\langle i_L \rangle_k$ and $\langle v_C \rangle_k$ are defined for all integer harmonic numbers k from $-\infty$ to $+\infty$. Since in practice it is not feasible to solve a set of infinite differential equations, an approximation is obtained by ignoring the harmonics larger than some nonnegative integer $N(-N \leq k \leq N)$. It is obvious that the larger N, the more Fourier coefficients are taken into account and i_L and v_c are reconstructed more accurately by their Fourier series.

2.6.3 Matrix representation

The set of differential equations in (2.31) restricted to $2N + 1$ Fourier coefficients can be described as,

$$\begin{aligned}
\frac{d}{dt} \langle I_L \rangle(t) &= (W - \frac{R_{load}r_C + R_{load}r_L + r_C r_L}{L(R_{load} + r_C)} I\ ) \langle I_L \rangle(t) - \frac{R_{load}}{L(R_{load} + r_C)} I\ \langle V_C \rangle(t) + Q_1 b \\
\frac{d}{dt} \langle V_C \rangle(t) &= \frac{R_{load}}{C(R_{load} + r_C)} I\ \langle I_L \rangle(t) + (W - \frac{1}{C(R_{load} + r_C)} I\ ) \langle V_C \rangle(t) \qquad (2.32)
\end{aligned}$$

where $\langle I_L \rangle(t)$ and $\langle V_C \rangle(t)$ are $n \times 1$ matrices with $n = 2N + 1$ and are defined as,

$$\langle I_L \rangle(t) = \begin{pmatrix} \langle i_L \rangle_{-N}(t) \\ \vdots \\ \langle i_L \rangle_{-1}(t) \\ \langle i_L \rangle_0(t) \\ \langle i_L \rangle_1(t) \\ \vdots \\ \langle i_L \rangle_N(t) \end{pmatrix} \quad \text{and} \quad \langle V_C \rangle(t) = \begin{pmatrix} \langle v_C \rangle_{-N}(t) \\ \vdots \\ \langle v_C \rangle_{-1}(t) \\ \langle v_C \rangle_0(t) \\ \langle v_C \rangle_1(t) \\ \vdots \\ \langle v_C \rangle_N(t) \end{pmatrix}$$

I is the $n \times n$ identity matrix, W is a $n \times n$ diagonal matrix with the imaginary numbers $+jN\omega_s$, $+j(N-1)\omega_s$, ...,$+j\omega_s$, 0,$-j\omega_s$, ..., $-j(N-1)\omega_s$, $-jN\omega_s$ on its diagonal,

$$W = \begin{pmatrix} +jN\omega_s & 0 & \dots & \dots & 0 \\ 0 & \ddots & & & \vdots \\ \vdots & & 0 & & \vdots \\ \vdots & & & \ddots & 0 \\ 0 & \dots & \dots & 0 & -jN\omega_s \end{pmatrix}$$

matrix b is a $n \times 1$ matrix with all components equal to $\frac{1}{L}V_d$,

$$b = \begin{pmatrix} \frac{1}{L}V_d \\ \vdots \\ \frac{1}{L}V_d \end{pmatrix}$$

and matrix Q_1 is a $n \times n$ diagonal matrix,

$$Q_1 = \begin{pmatrix} \langle q \rangle_{-N} & 0 & \dots & \dots & 0 \\ 0 & \ddots & & & \vdots \\ \vdots & & \langle q \rangle_0 & & \vdots \\ \vdots & & & \ddots & 0 \\ 0 & \dots & \dots & 0 & \langle q \rangle_N \end{pmatrix}.$$

In the open loop situation, the switching function q is periodic in time with period of T_s and it can be easily computed that $\langle q \rangle_0 = d$ and $\langle q \rangle_k = \frac{1}{2\pi kj}(1 - e^{-2\pi kjd})$ for all integer $k \neq 0$.

Equation (2.32) can be compactly written as,

$$\frac{d}{dt}X(t) = AX(t) + QB \tag{2.33}$$

where the vector $X(t)$ (a vector of dimension $(4N+2) \times 1$) is defined by,

$$X(t) = \begin{pmatrix} \langle I_L \rangle(t) \\ \langle V_C \rangle(t) \end{pmatrix}.$$

The matrix A, Q and vector B are defined as,

$$A = \begin{pmatrix} W - \frac{R_{load}r_C + R_{load}r_L + r_C r_L}{L(R_{load}+r_C)} I & -\frac{R_{load}}{L(R_{load}+r_C)} I \\ \frac{R_{load}}{C(R_{load}+r_C)} I & W - \frac{1}{C(R_{load}+r_C)} I \end{pmatrix}, \quad Q = \begin{pmatrix} Q_1 & 0 \\ 0 & 0 \end{pmatrix}, \quad B = \begin{pmatrix} b \\ 0 \end{pmatrix}$$

with 0's in Q and B being appropriate zero submatrices.

It is proven in [10] that matrix A is invertible and the differential equation (2.33) has one stable equilibrium solution, given by $X = -A^{-1}QB$. This solution gives the state variables in open loop situation upto N harmonics.

For the closed loop converter, the switching function $q(t)$ is based on feedback of the state variables. This makes the differential equations (2.31) to be no longer linear as they are in open loop situation [10]. So the computations for closed loop situations are even more complicated than they are in open loop situation and the case of just gain proportional control is considered in [10] and extended to constant state feedback control without integral action.

The Fourier series model can be considered as a generalized form of state-space averaging technique. It can predict all behaviours that the small signal model does and in addition to the averages of i_L and v_C, the shape of the signals over an entire period can be computed from the Fourier coefficients in the solution vector X. The model is frequency-dependent which is an improvement with respect to simple state-space averaging of Section 2.2. But the disadvantage of the model is high order matrix calculations and the assumption that the converter stays in one mode of operation only is made in its derivation.

The Fourier series model presented in this section, models the system in continuous-conduction mode. Using the same method, a model can be derived for converters working in discontinuous-conduction mode. But the Fourier series model cannot handle the system when it switches back and forth between continuous-conduction mode and discontinuous-conduction mode.

A numerical example of the Fourier series model will be discussed in Chapter 4.

2.7 Circuit simulation tools

General circuit simulation packages can also be used to simulate the buck converter. Here, two available tools (PSpice and MATLAB/Simulink) are studied. In open loop situation, PSpice gives a transient response very similar to C-code simulation results. But as the circuit gets more complicated, for instance in closed loop situations with PI control, PSpice shows numerical errors that make it difficult to get the real behaviour of the system.

Alternatively, the power electronics toolbox in MATLAB/Simulink package contains components like MOSFETs and diodes with optional characteristics. By entering the characteristics of the components from their datasheet, the blocks will act close to the real MOSFET or Diode and power electronic circuits can be simulated using this tool.

2.8 Conclusion

Some of the methods for modeling the buck converter are introduced. The models can be divided into linear and non-linear models. The linear models, that includes small signal model and linearized discrete model, assume that system is working around a particular operating point that naturally requires the converter to be modeled either in continuous-conduction mode or in discontinuous-conduction mode. Having a linear model that predicts the behaviour of the system in both modes of operation is not possible and the linear models are effective only for very small variations around the operating point.

The nonlinear models, that includes C-code simulation which is implemented for this work, PSpice simulation and Simulink, simulate the system accurately by considering very fine time-steps and calculating states of the system at each time step. So, both mode of operations are possible but these models get numerically involved with the details of the converter and are time-consuming and cannot be used for analytical studies.

There are models based on Fourier series that despite being complicated, considers the converter to be either in continuous-conduction mode or discontinuous-conduction mode. These models provide better ripple computations with respect to the models mentioned before but do not show the behaviour of the converters when it switches between the two modes.

The large signal model developed in this thesis in Section 2.3 overcomes the limitations by predicting the behaviour of the system in both modes of operation and has the advantages of the nonlinear models but is parsimonious.

In the next chapters, the behaviour of the models are considered through simulations and experimental results.

Chapter 3

Frequency-response analysis of the buck converter

In this chapter, some of the models discussed in Chapter 2 are used for a particular buck converter to predict behavior in terms of frequency-response. The predicted results are compared with experimental results. The simulations and experiments are done using two different experimental buck converter prototypes (Buck1 and Buck2 with parameters in Appendix A), but the results are presented for Buck2 as similar accuracy is obtained for Buck1.

3.1 C-code simulation and experimental frequency-responses

In this section, the frequency-response of the buck converter is obtained experimentally and compared with the frequency-response from simulations with C-code. The comparison results in estimating the equivalent series resistance (ESR) of the capacitor in the buck converter.

The experimental setup to obtain the frequency-response is provided in Appendix A. The input signal to the experimental buck converter, given in (3.1), consists of a dc voltage V_{dc} plus a sinusoidal signal of amplitude A and frequency f. The dc voltage is adjusted such that it provides the desired output voltage (*i.e.* it keeps the system working at the desired operating point). The amplitude of the sinusoidal signal is kept constant at $A = 1$V while its frequency f is varied over a certain range and the resulting response on the output voltage is collected and processed to provide the frequency-response.

$$V_{in} = V_{dc} + Asin(2\pi ft) \qquad f = 200\text{Hz to } 10\text{kHz} \tag{3.1}$$

The frequency-response of the C-code simulation model is obtained using the same input given in (3.1) with $A = 1$V. Figure 3.1 shows the comparison between the experimental

and C-code simulation model frequency-responses for Buck2 with parameters given in Appendix A but with $r_C = 0$. It can be seen that the two responses do not match well.

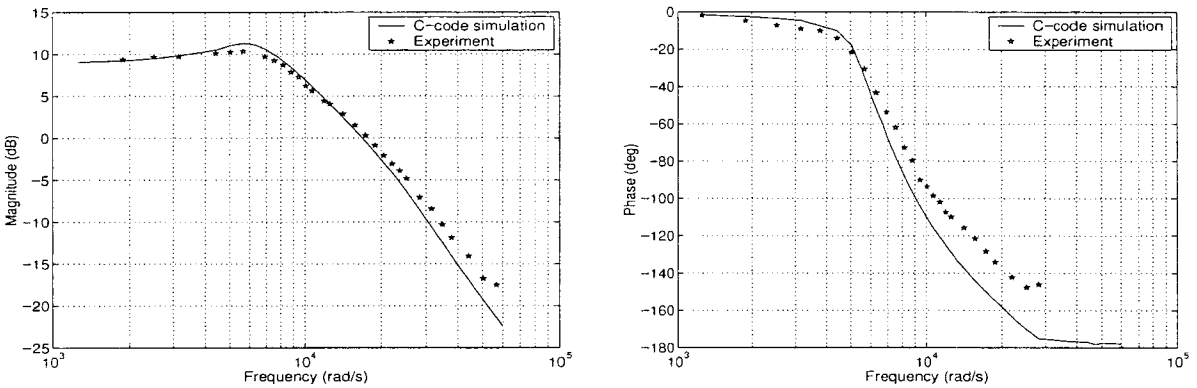

Figure 3.1: Magnitude and phase frequency-responses for Buck2 with $r_C = 0$

3.1.1 Equivalent series resistance (ESR) of capacitor

Since the values of all variables in the C-code simulation model has been chosen exactly equal to the component values of the experimental setup, the reason for mismatch in the frequency-responses discussed in the previous section, could be due to the ESR of capacitor. In the real system ESR exists while it has not been considered in this C-code simulation with results in Figure 3.1. ESR of capacitor, denoted by r_C in Section 2.1, is not easily measurable. So, using C-code simulation model, the frequency-response is obtained for different values of r_C and is compared with the experimental frequency-response. For a particular value of r_C simulation results match the experimental results and this value is chosen as the ESR of the capacitor. Figure 3.2 compares the frequency-response of Buck2 obtained from C-code simulation considering $r_C = 0.2\Omega$ and the experimental frequency-response.

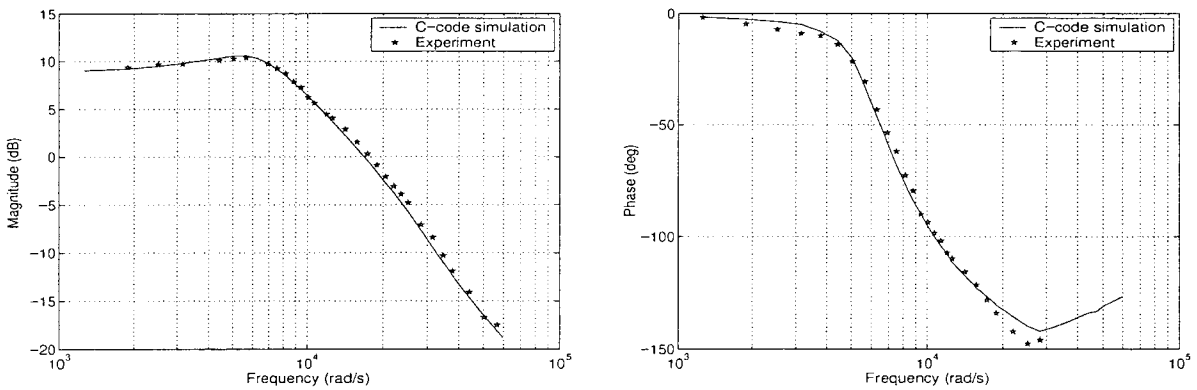

Figure 3.2: Magnitude and phase frequency-responses for Buck2 with $r_C = 0.2\Omega$

It can be seen that two frequency-responses are better-matched compared to the case with $r_C = 0$.

Buck1 prototype has the same type of capacitor but different inductor. Hence C-code simulations are repeated for Buck1 with parameters given in Appendix A and it is confirmed that with this value of ESR $r_C = 0.2\Omega$ obtained for Buck2, the C-code simulation results agrees with the experimental results for the Buck1 converter. Figures 3.3 and 3.4 show the frequency-response of Buck1 in comparison with C-code simulations considering $r_C = 0$ and $r_C = 0.2\Omega$ respectively.

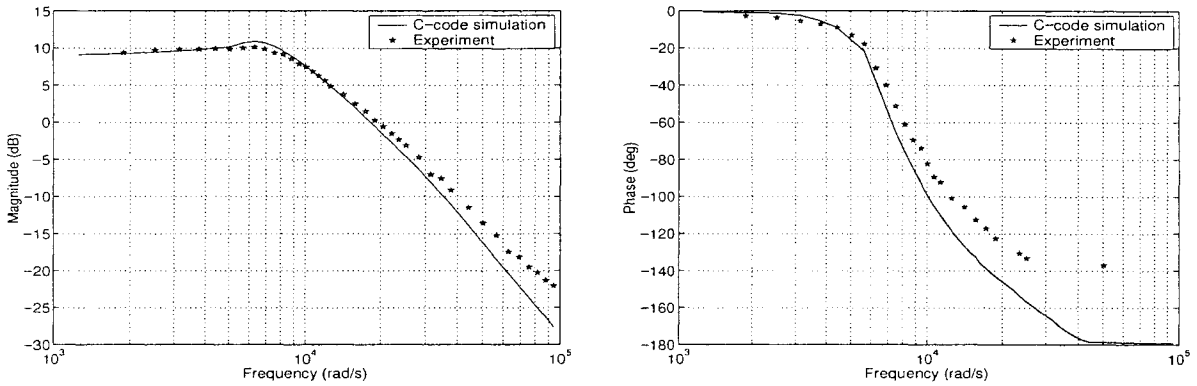

Figure 3.3: Magnitude and phase frequency-responses for Buck1 with $r_C = 0$

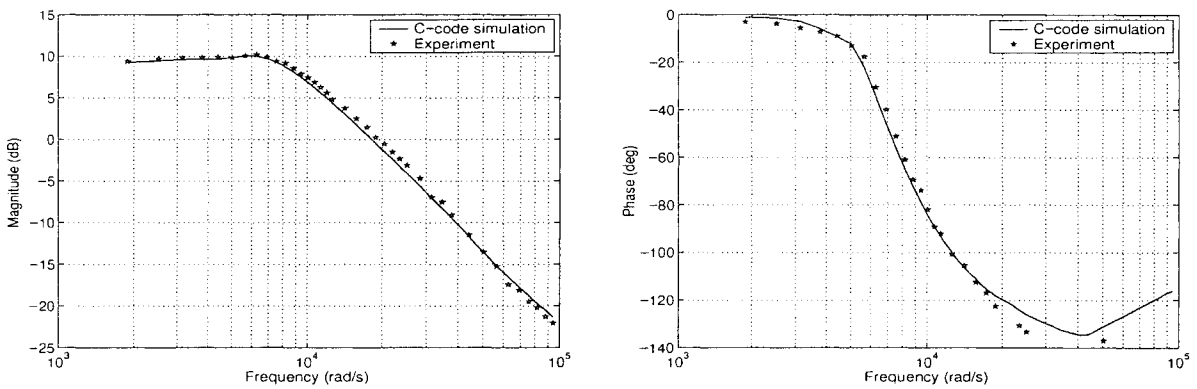

Figure 3.4: Magnitude and phase frequency-responses for Buck1 with $r_C = 0.2\Omega$

3.2 Frequency-response of large signal model

In this section, the frequency-response obtained from the large signal model of Section 2.3 with the input signal given in (3.2) and with the amplitude of sine-wave $A = 1$V, is obtained and compared with the frequency-response of the C-code simulation with the

input given in (3.1) and with the amplitude of sine-wave $A = 1$V. These results (Figures 3.5 and 3.6), shows the need for a zero order hold compensation for the large signal model in the obtained frequency-response.

$$V_{in_k} = V_{dc} + Asin(2k\pi fT_s) \qquad f = 200\text{Hz } to \text{ } 10\text{kHz} \tag{3.2}$$

The input signal in (3.2) can be written in terms of duty cycle as,

$$d_k = d_0 + d_1 \sin(k\omega T_s) \tag{3.3}$$

where $d_k = \frac{V_{in_k}}{\hat{V}_{st}}$, $d_0 = \frac{V_{dc}}{\hat{V}_{st}}$ and $d_1 = \frac{A}{\hat{V}_{st}}$.

As Figures 3.5 and 3.6 show, the simulated and the large-signal model based frequency-responses do not match well especially at high frequencies in phase.

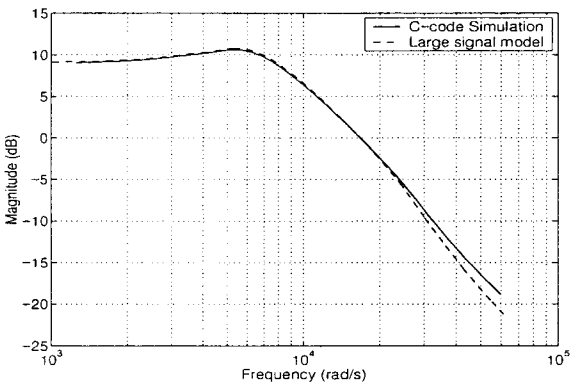

Figure 3.5: Magnitude of frequency-response

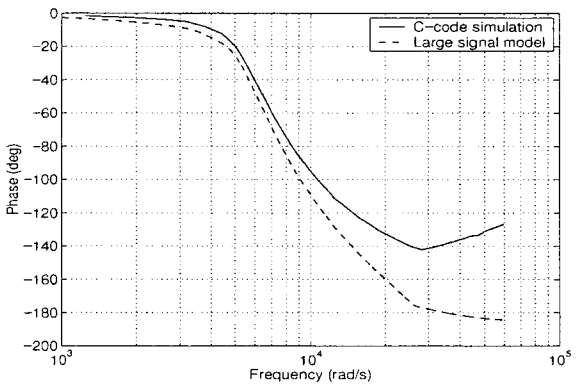

Figure 3.6: Phase of frequency-response

The frequency-response obtained from large signal model is a discrete frequency-response. For the large signal model, the switching frequency f_s is considered as sampling rate so according to the sampling rate theorem, the discrete frequency-response is valid upto a maximum frequency of $\frac{f_s}{2}$Hz or $\frac{\pi}{T_s}$ rad/s [3].

For Buck2, the switching frequency (*i.e.* sampling frequency for large signal model) is $f_s = 30$kHz. Based on the sampling theorem, for Buck2 the highest frequency up to which the large signal model is valid is $\omega_h = 15$kHz ($15\text{k} \times 2\pi \simeq 10^5$ rad/sec). Even though the frequency-responses in Figures 3.5 and 3.6 are plotted within the range of this frequency ω_h, there is an aliasing error due to the higher-frequency components present in the system, which is the reason for the discrepancy that can be seen at higher frequencies in magnitude and phase plots of the frequency-response. Some of this error is also due to the phase and magnitude error introduced by the ZOH assumption made in the discrete time modeling and is next compensated for.

3.3 Zero-order hold

Zero-order hold is one of the methods used for approximation of a continuous signal $f(t)$ from the discretized signal $f(kT)$, where T is the sampling period and k is the sample number. Zero-order hold accepts a sample $f(kT)$ at $t = kT$ and holds it until the next sample $f((k+1)T)$ arrives at $t = kT + T$. In the large signal model, the conversion from continuous-time to discrete-time is done assuming zero-order hold on duty cycle. So the effect of the zero-order hold on the frequency-response of large signal model is studied in this section.

3.3.1 Transfer function of the zero-order hold

In time-domain a zero-order hold can be given by the following piecewise function,

$$f_k(t) = f(kT), \qquad kT \leq t < (k+1)T$$

. The impulse response $h(t)$ of the zero-order hold is expressed as,

$$h(t) = u(t) - u(t-T) \tag{3.4}$$

where $u(t)$ is the unit-step function.
The transfer function of the zero-order hold is obtained by taking the Laplace transform of (3.4),

$$H(s) = \frac{1}{s} - \frac{e^{-sT}}{s}. \tag{3.5}$$

Replacing s by $j\omega$ in (3.5), this frequency-response of ZOH can be obtained as,

$$H(j\omega) = \frac{1}{j\omega} - \frac{e^{-j\omega T}}{j\omega} = \frac{e^{-\frac{j\omega T}{2}}(e^{\frac{j\omega T}{2}} - e^{-\frac{j\omega T}{2}})}{j\omega} = Te^{-\frac{j\omega T}{2}} \frac{sin(\frac{\omega T}{2})}{\frac{\omega T}{2}}. \tag{3.6}$$

3.3.2 Frequency-response of the sampled signal

The transfer function given in (3.6) is continuous, but in order to use it as a compensation of the frequency-response of the discretized model, sampled function should be used. In this section, the relation between the frequency-response of a continuous signal and the frequency-response of a sampled signal is obtained [3].
An ideal sampling function represents a train of unit impulses and can be defined as,

$$\delta_T(t) = \sum_{n=-\infty}^{\infty} \delta(t - kT)$$

where T is the uniform sampling period.
Assuming $f(t)$ as the continuous signal and $f^*(t)$ as the discrete signal resulting from sampling,

$$f^*(t) = f(t)\delta_T(t). \tag{3.7}$$

The impulse train $\delta_T(t)$ is expanded in a complex Fourier series and combined with (3.7) resulting in,

$$f^*(t) = \frac{1}{T} \sum_{n=-\infty}^{\infty} f(t) e^{jn\omega_s t} \tag{3.8}$$

where $\omega_s = \frac{2\pi}{T}$.
Taking the Laplace transformation of (3.8) and replacing s with $j\omega$, the frequency-response of $f^*(t)$ is obtained as,

$$F^*(j\omega) = \frac{1}{T} \sum_{n=-\infty}^{\infty} F[j(\omega + n\omega_s)]. \tag{3.9}$$

By passing $F^*(j\omega)$ through an ideal lowpass filter $H(j\omega)$ given by,

$$H(j\omega) = \begin{cases} 1, & |\omega| \leq \omega_s/2 \\ 0, & |\omega| > \omega_s/2 \end{cases}.$$

The base band frequency-response characteristics are obtained in the absence of aliasing as,

$$F^*(j\omega) = \frac{1}{T} F(j\omega) \tag{3.10}$$

which is the same as (3.9) with $n = 0$.
(3.10) shows the relation between frequency-response of continuous signal $F(j\omega)$ and frequency-response of the sampled signal $F^*(j\omega)$ in this base band.

3.3.3 Zero-order hold compensation

By combining (3.6) that represents the continuous frequency-response of the zero-order hold, with (3.10), the frequency-response of the sampled zero-order hold signal is obtained in absence of aliasing as,

$$H^*_{ZOH}(j\omega) = \frac{1}{T} H(j\omega) = e^{-\frac{j\omega T}{2}} \frac{sin(\frac{\omega T}{2})}{\frac{\omega T}{2}} \tag{3.11}$$

in this base band.

It can be seen that if the sampling period T is very small the zero-order hold amplitude will be very close to '1' and its phase will be very close to '0'. In other words the zero-order hold will have almost no effect on the frequency-response of the discretized system. But for bigger values of sampling period T, the zero-order hold will have some noticeable magnitude and phase that will affect the frequency-response of the discretized system. It is obvious from (3.11) that the changes introduced by zero-order hold in the frequency-response of the discretized system is more apparent at higher frequencies.

3.4 ZOH-compensated large signal model

If the discrete-time frequency-response obtained in Section 3.2 is denoted $G_d(e^{j\omega T_s}, d_0, d_1)$, the ZOH compensated continuous time frequency-response $G(j\omega, d_0, d_1)$ is given from 3.10 as,

$$G(j\omega, d_0, d_1) = G_d(e^{j\omega T_s}, d_0, d_1)\frac{\omega T_s/2}{\sin(\omega T_s/2)}e^{j\omega T_s/2}. \tag{3.12}$$

Figure 3.8 and 3.7 show the compensated magnitude and phase of the frequency-response of the large signal model compared with C-code and experimental results respectively. As shown in the figures, adding the compensation improves the frequency-response of the discretized system.

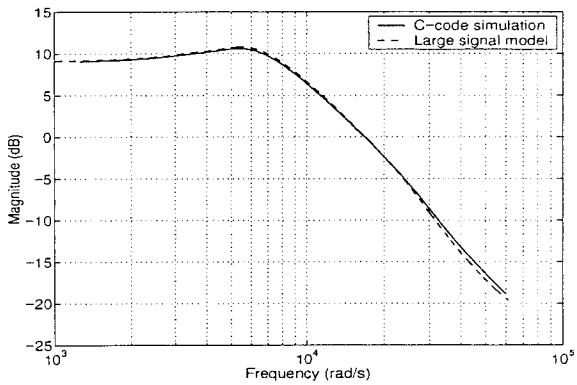

Figure 3.7: Compensated magnitude of frequency-response

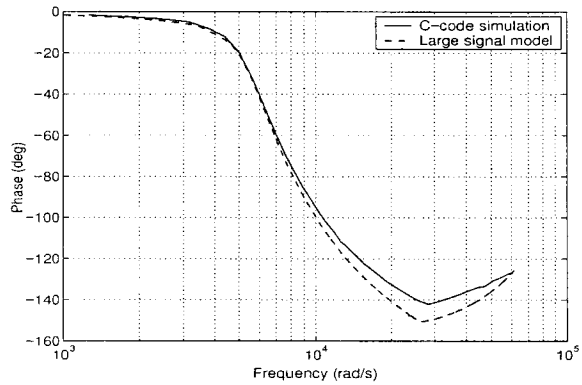

Figure 3.8: Compensated phase of frequency-response

It can also be seen that even after compensation there are still some error at higher frequencies, specially in phase plot, due to aliasing. This problem will be reduced at higher switching frequencies (*i.e.* higher sampling periods). For the experimental setup of Buck2, the switching frequency is $f_s = 30$kHz and in practice buck converters are often designed for higher switching frequencies.

3.5 Nonlinear behavior of the buck converter

The frequency-response of Buck2 is obtained using C-code simulation, with an input signal given by Equation (3.1) with $A = 1$V, which corresponds to variations of ± 0.1 in duty cycle. Even though this variation in duty cycle is quite small, compared to the operating point of 0.7177 (variations of 13.93%) Figures 3.9 and 3.10 show this frequency-response does not agree with the small signal frequency-response obtained from (2.9).

This shows the nonlinear behavior of the buck converter and shows that the small signal transfer function can represent the system only for very small variations of duty cycle around the operating point. This is investigated further below.

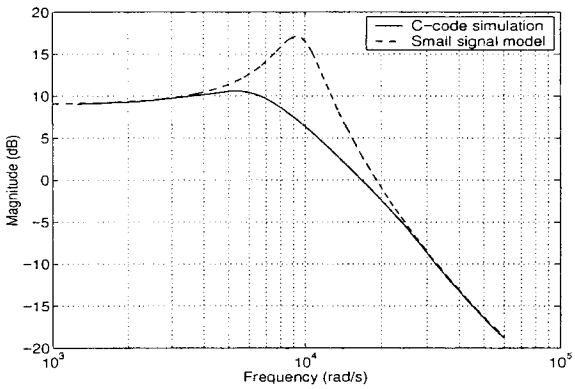

Figure 3.9: Magnitude of frequency-response

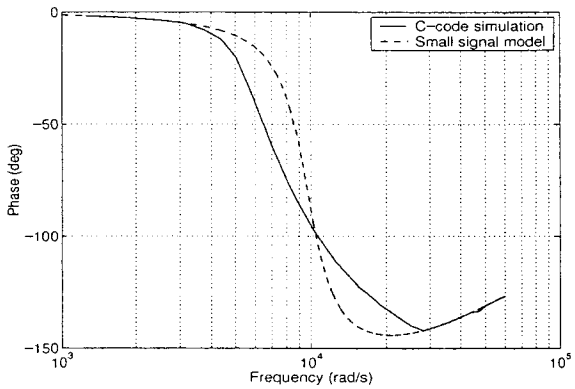

Figure 3.10: Phase of frequency-response

3.5.1 Linear region

To find out where the system starts exhibiting behaviour not predicted by the small signal frequency-response, the converter is simulated with different amplitudes of input sine-wave. As long as the system operates in continuous-conduction mode, the frequency-response of the system does not depend on the amplitude of sinusoidal input and will remain the same for all the amplitudes. But as soon as the system starts working in continuous and discontinuous mode at a certain frequency and certain amplitude of input duty cycle, the frequency-response will no longer be the same as the small signal (state-space averaged) frequency-response.

To give a numerical example, for the Buck2 parameters operating at a dc output voltage of 20V, with $d_0 = 0.7177$, the small signal model is valid for duty cycle changes of $|d_1| \leq 0.0166$ around a dc value of $d_0 = 0.7177$. This is a region of validity of approximately 2.3% changes in the duty cycle.

3.5.2 Large signal model

The nonlinear behaviour of buck converter can also be predicted by the large signal model. The input duty cycle of (3.3) is given to the large signal model of Equations (2.10) and (2.11). A plot of the magnitude and phase frequency-response for three values of d_1 at a fixed d_0 obtained using (3.12) with the experimental frequency-response measured on a Buck2 is shown in Figures 3.11 and 3.12.

The smallness of $d_1 = 0.01$ presents considerable difficulty in measuring the frequency-response in the presence of ripple and noise in the experimental system in this region. This is the main source of error in Figures 3.11 and 3.12 at this small d_1.

Although not clear from Figures 3.11 and 3.12, it is interesting to note that for a given d_1 beyond the small signal limit ($|d_1| > 0.0166$ for Buck2), the converter behaviour changes

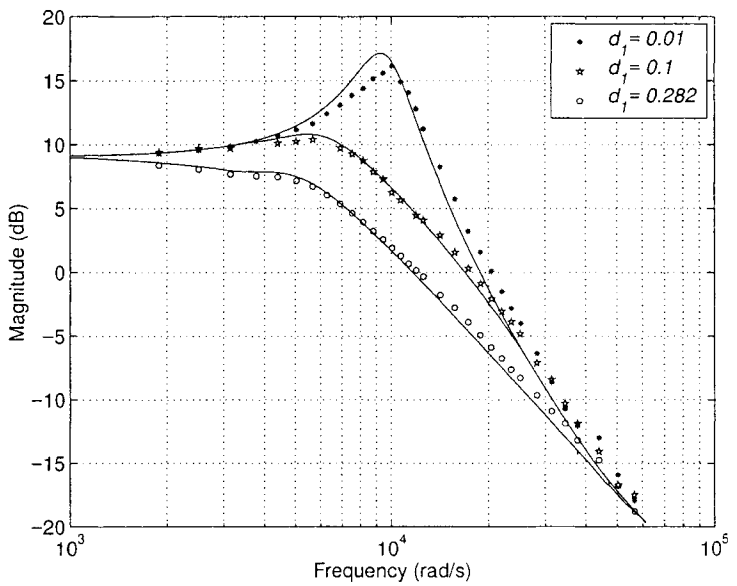

Figure 3.11: Magnitude of frequency-response for large signal model and experiment

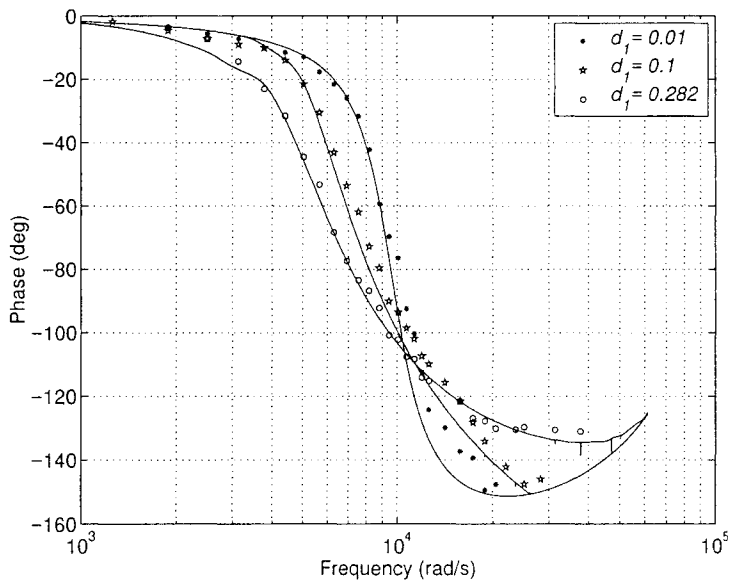

Figure 3.12: Phase of frequency-response for large signal model and experiment

from being entirely in continuous-conduction mode at low frequencies region to behaviour with continuous and discontinuous conduction modes at higher frequencies. The frequency of this transition from exclusive continuous mode to mixed modes decreases with increasing amplitude (d_1) in the model as well as in experiment. The presence of continuous and discontinuous modes in any given frequency-response for fixed d_1 precludes the use of simpler methods of computation of the large signal frequency-response.

3.6 Newton-Raphson technique to compute frequency-response

The frequency-response of the large signal model at a frequency is obtained by comparing the magnitude at that frequency in the output voltage and its phase shift with the input sinusoid. But this way of computation is rather a time consuming process since it needs to be done at each frequency. An alternative faster method is using Newton-Raphson technique. A periodic steady-state vector of state variables at the start of the sinusoidal cycle is computed by Newton-Raphson type numerical method. A modification of the method in [15] with numerical computation of the required Jacobian [18] serves to compute this periodic steady-state state vector. Convergence of the computation to obtain the periodic steady-state state vector is attained within a maximum of 5 iterations of the Newton-Raphson method. It is to be noted that this accelerated numerical technique of computation presupposes that the ratio of the frequency $\frac{\omega}{2\pi}$, at which the response is sought to the switching frequency $\frac{1}{T_s}$ is a ratio of rational numbers. A more detailed explanations of Newton-Raphson method is given in Appendix C.

3.7 Frequency-response of the linearized discrete model

The frequency-response of the linearized discrete model (Section 2.5.2) is computed for Buck2 (Appendix A) and is compensated using ZOH compensation method (3.12).

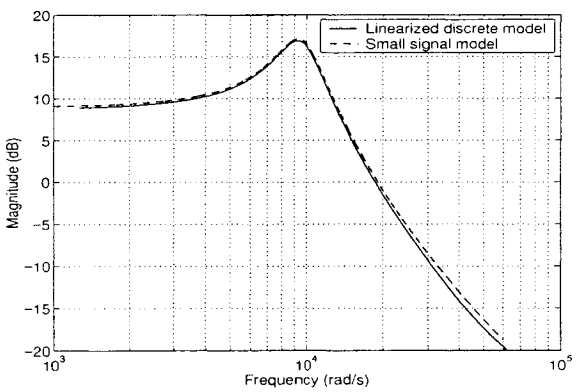

Figure 3.13: Magnitude of frequency-response

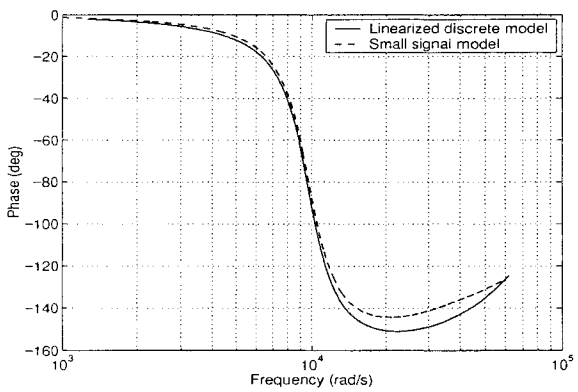

Figure 3.14: Phase of frequency-response

As Figures 3.13 and 3.14 show the results are similar to the frequency-response of the state space small signal model in the literature. Since the linearized discrete model assumes that system works only in continuous-conduction mode, it does not give any more information about the system than small signal model gives and basically it is just another form of linearizing the buck converter system. However it takes into account the operating point value of d better.

From Equation (2.9) it can be seen that the frequency-response of small signal model is not dependent on the operating point. But as (2.28) shows, the frequency- response of linearized discrete model is dependent on the operating point. Figures 3.15 and 3.16 shows the frequency-response of linearized discrete model for Buck2 with different values of output voltage V_0. The main conclusion is that from a controller design point of view, the continuous-conduction state space averaged small signal model adequately captures the relevant information for design.

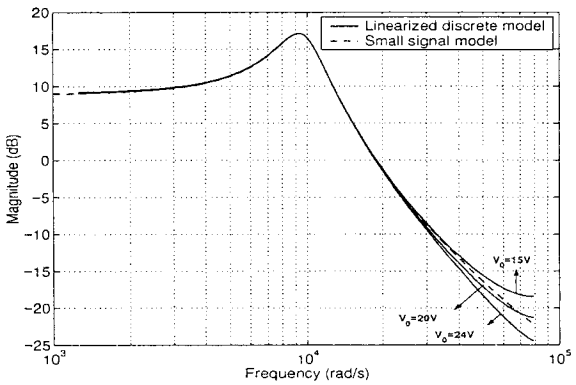

Figure 3.15: Magnitude of frequency-response for different operating points

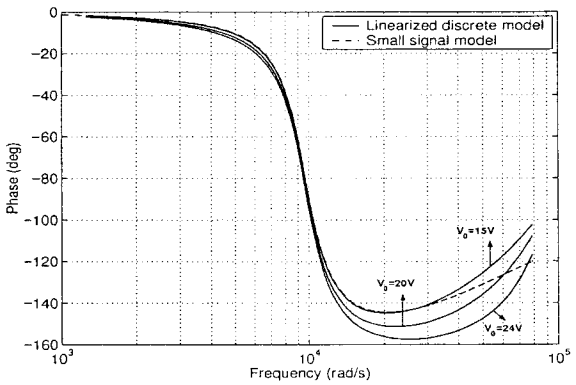

Figure 3.16: Phase of frequency-response for different operating points

3.8 Conclusion

The study on frequency-response concludes that it is essential to consider the values of parasitic parameters r_C and r_L in simulations, because as shown, their effect on buck converter behaviour is significant.

For the discretized models (which includes large signal model and linearized discrete model), compensation for ZOH is necessary, due to the low switching rate used in this work, particularly for phase response.

By studying the frequency-response obtained from large signal model for different values of d_1, it is shown that the amplitude d_1, the dc bias d_0 and the frequency ω in (3.3), affect the entry into discontinuous-conduction mode from continuous-conduction mode

and vice versa. Models designed only for one particular mode of operation (continuous or discontinuous), cannot fully predict the system's behaviour. Also, since the frequency-response is in general a function of d_0, d_1 and ω, the linearized models that consider the frequency-response to be independent of d_1, are only valid for very small variations in d_1 typically in the 2% range.

Chapter 4

Prediction of limit cycles and ripple

4.1 Stability limit

The stability limit for PI controller gains of a buck converter is the value of gains at which the system gets into and exhibits sustained oscillatory behaviour (limit cycles). Knowing these stability limits of the buck converter is important for the prediction of limit cycles. To determine the stability limits, besides simulations from the models, an experimental setup of the buck converter with a PI controller is implemented. The circuit diagram of the experimental setup and the explanations of the circuit are given in Appendix B.

4.1.1 Finding stability limit gains

The stability limit gains are found in the following ways,

- From the experimental setup, the value of the proportional gain K_p is kept constant and the integral gain K_i is increased to the point that the system shows a limit cycle behavior. The experiment is repeated for a range of $0 \leq K_p \leq 1$. The plot of K_i versus K_p gives the region of stability. Due to some variability in K_i observed when doing the experiment, the trials are repeated for each K_p a few times and the average of the K_i's so obtained is considered to determine the stability region.

- From state space averaged small signal model (Section 2.2), the stability region is obtained for each value of K_p and K_i that leads to closed loop poles on the $j\omega$ axis.

- From C-code simulation, K_p is kept constant and K_i is increased. For each K_i value the steady-state inductor current is checked. If the inductor current enters into discontinuous mode, then K_i is considered as the limit of stability. This is because for the parameters of Buck2, in steady-state, the converter works in continuous-conduction mode. But if due to oscillations the variations in duty cycle increase, the converter is pushed to continuous and discontinuous modes of operation. Once it reaches the discontinuous mode then the damped frequency-response (Figures 3.11 and 3.12) stabilizes the system.

The stability region obtained from the small signal model matches the one obtained from C-code simulations and both match well with the experimentally obtained stability region. This stability region is shown in Figure 4.1. It can be seen that by increasing the value of K_p, a higher value of K_i is needed to make the buck converter system unstable.

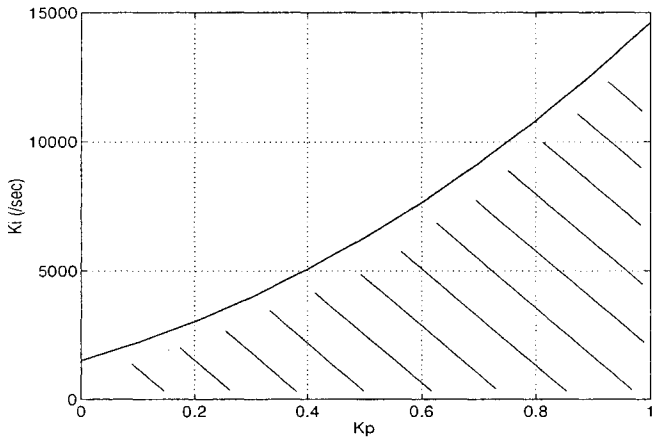

Figure 4.1: Stability region

4.2 Prediction of limit cycles from large signal model

Limit cycle oscillations happen when the buck converter switches back and forth between two modes of operation, continuous and discontinuous conduction. Since large signal model considers both modes of operation, it can predict the limit cycles (frequency and amplitude of oscillations). In order to predict the limit cycles of the buck converter, from large signal model, the Nyquist stability criterion is used. According to this criterion, the system $G(j\omega, d_0, d_1)$ computed in Section 3.4 using large signal model of (2.10) and (2.11) in Section 2.3 with an analog PI controller $C(j\omega)$ is considered to be oscillating if,

$$G(j\omega, d_0, d_1) = -\frac{1}{C(j\omega)}. \tag{4.1}$$

Assuming sinusoidal oscillations, it is seen from Figures 3.11 and 3.12 that the frequency-response of the buck converter during oscillation depends on the amplitude of oscillations (d_1). So, in order to solve the Equation (4.1) for frequency and amplitude of oscillation, the frequency-response of $G(j\omega, d_0, d_1)$ for different amplitudes of input sinusoid is obtained and compared with the frequency-response of $-\frac{1}{C(j\omega)}$.

As the example in Figure 4.2 shows, out of three points of intersection between the two bode plots of $G(j\omega, d_0, d_1)$ and $-\frac{1}{C(j\omega)}$, only one intersection happens at the same frequency for both magnitude and phase plots. This frequency is considered as the oscillation frequency and the corresponding amplitude as amplitude of oscillation. For this

example, PI controller $C(j\omega)$ is considered with the controller gain values of $K_p = 0.1$ and $K_i = 2.214$/ms. The amplitude of output voltage oscillations of the converter, d_1 and the frequency of oscillation are obtained from Figure 4.2 as 1.05V, 0.02318 and 1790Hz respectively.

From the small signal model, the upper limit of K_i gain for stability of the closed loop with $K_p = 0.1$ is 2.214/ms. For this value, the frequency of oscillation for the poles on the $j\omega$ axis predicted by the state space small signal model is 1810Hz. Experimental measurements with $K_p = 0.1$ and $K_i = 2.214$/ms indicates a frequency of oscillation of 1916Hz and an amplitude of oscillation of output voltage of 1.0231V for the limit cycles.

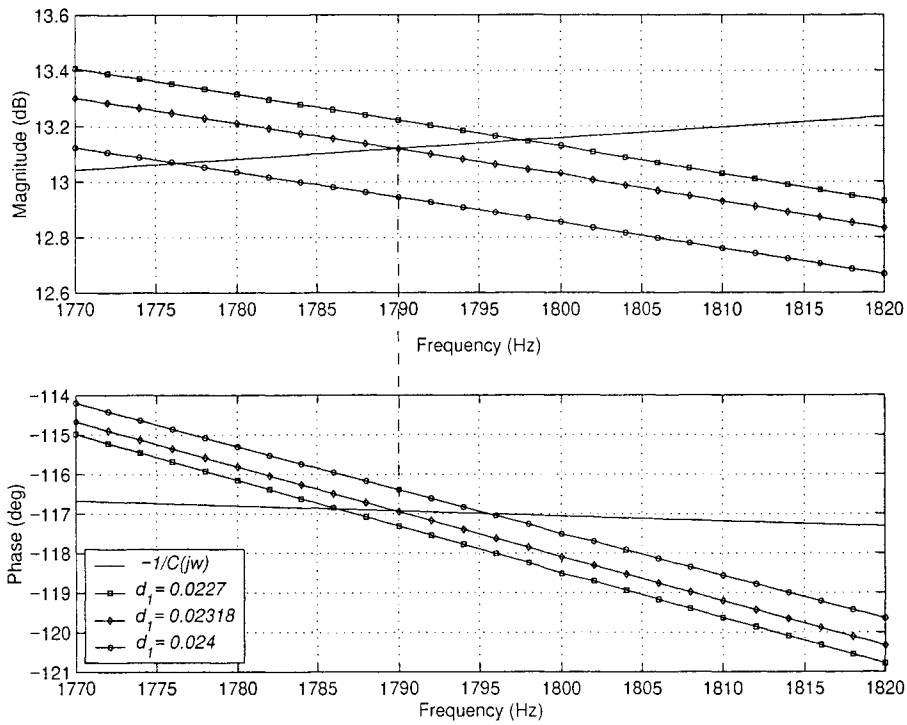

Figure 4.2: Magnitude and phase frequency-responses of right hand side and left hand side of (4.1)

In Figure 4.3 a plot of amplitude and frequency of limit cycles as predicted by this approach for a range of K_p and K_i along with experimental results is shown. In Figure 4.3, for each K_p gain, the K_i gain is always set to the stability limit value predicted by the small signal state-space averaged model. From Figure 4.3 the error between the predicted and experimental results is within 5% for the amplitude of oscillations and within 8% for the frequency of oscillations. The source of error between experimental and the computed results are in the assumptions made for developing the large signal model. In developing this model the diode and switch are considered ideal, parasitics of the experimental system due to wiring and layout are not considered and passive components are considered linear, time-invariant and frequency independent.

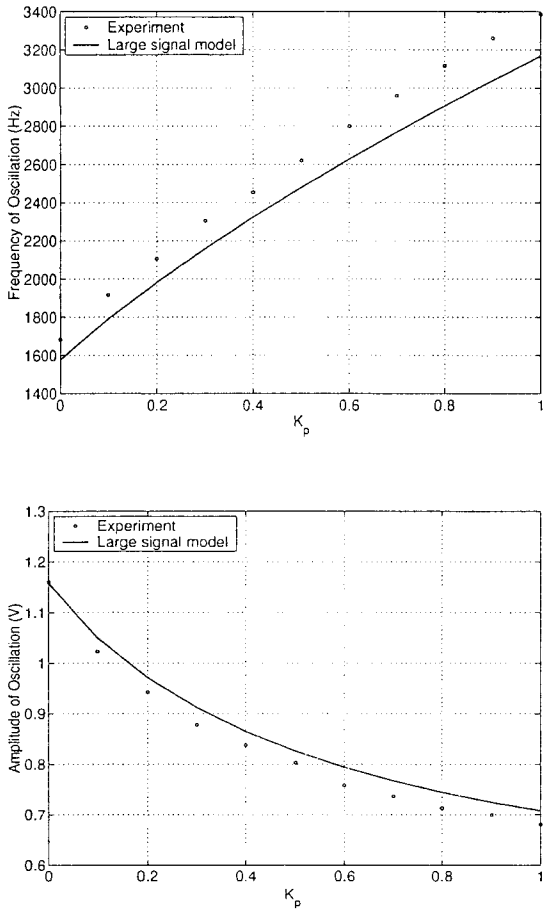

Figure 4.3: Output voltage amplitude and frequency of oscillations of limit cycles versus K_p gain - from large signal model and experiment

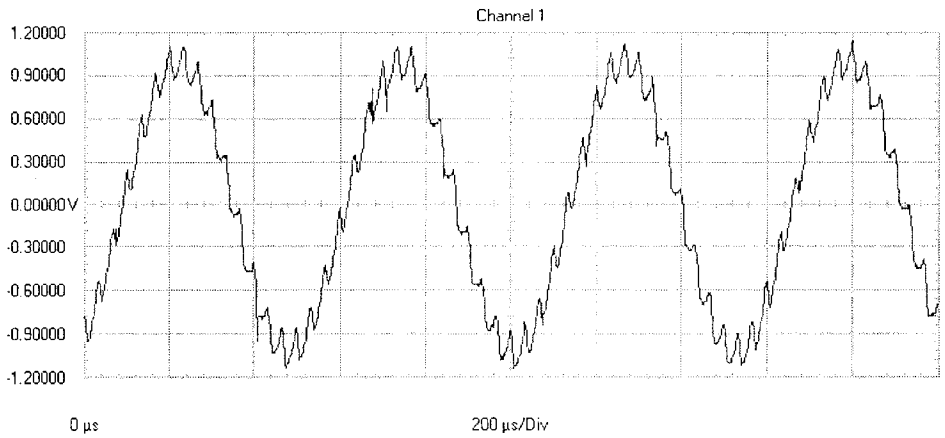

Figure 4.4: Oscillation in output voltage - from experiment

Figure 4.4 shows the oscillations of output voltage from the experimental system with a K_p gain of 0.1 and K_i gain of 2.214/ms. Barring high frequency switching, this waveform is sinusoidal indicating the validity of the assumption of sinusoidal oscillations made in Section 4.2.

4.2.1 Stability of limit cycles

When the system of a closed loop buck converter starts to oscillate, for example due to an increase in controller gains, and the amplitude of the oscillation gets larger, Figures 3.11 and 3.12 show the frequency-response of the system is pushed to a more damped behaviour. The damped frequency-response, causes the system to be stable, so the amplitude of oscillations reduces and consequently the frequency-response of the system is shifted to under-damped behaviour predicted by small signal model. With under-damped frequency-response, the amplitude of oscillations in system increases again. This phenomenon guarantees the stability of the limit cycles. It also shows that the edge of stability in a closed loop buck converter can be well predicted from the small signal model. But the amplitude of oscillations of limit cycles because of the presence of both continuous and discontinuous modes requires the large signal model.

4.3 Steady-state behaviour and ripple

In this section the steady-state behaviour of the buck converter is predicted from the large signal model and compared with the experimental results. From the equations of the large signal model,

$$x_{(k+d_k)T_s} = F_1 x_{kT_s} + G_1 V_d \tag{4.2}$$

$$x_{(k+1)T_s} = F_3 F_2 x_{(k+d_k)T_s} \tag{4.3}$$

and by substituting $x_{(k+d_k)T_s}$ from Equation (4.2) into Equation (4.3),

$$x_{(k+1)T_s} = F_3 F_2 F_1 x_{kT_s} + F_3 F_2 G_1 V_d. \tag{4.4}$$

Since in steady-state, $x_{(k+1)T_s} = x_{kT_s}$, so Equation (4.4) can be written as,

$$x_{kT_s} = F_3 F_2 F_1 x_{kT_s} + F_3 F_2 G_1 V_d$$

that gives the periodic steady-state state variables as follows,

$$x_{kT_s} = (I - F_3 F_2 F_1)^{-1} F_3 F_2 G_1 V_d. \tag{4.5}$$

In order to calculate the steady-state variables x_{kT_s}, the operating point duty cycle should be known and also it is necessary to know if, in steady-state, the system is working in continuous-conduction mode or discontinuous-conduction mode.

Using the periodic boundary condition state variables x_{kT_s} as initial conditions, the state variables in between switching periods can be computed. As an example, for Buck2 with parameters given in Appendix A, the state variables in between switching periods are computed by discretizing Equation (2.3) during the switch on time and during switch off time with small time steps (*e.g.* time steps of $\frac{dT_s}{100}$ and $\frac{(1-d)T_s}{100}$). Considering x_{kT_s} as initial conditions, the state variables at each time step are calculated. The result of such computation for Buck2 with $V_0 = 20\text{V}$, $I_L = 2\text{A}$ and $D = 0.7177$ is shown in Figure 4.5.

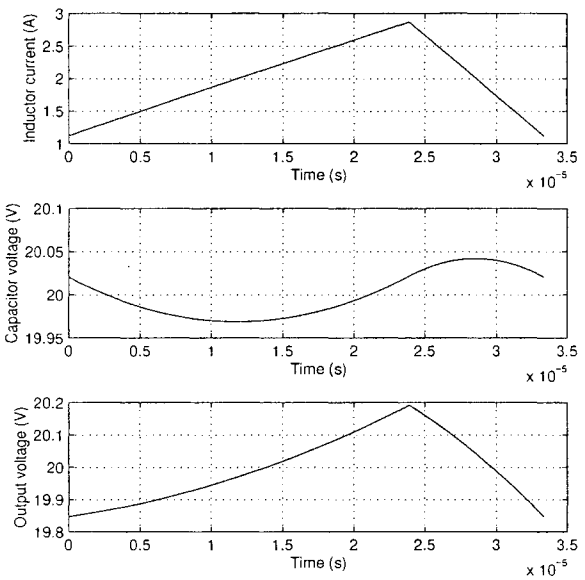

Figure 4.5: Steady-state values for one switching period obtained from large signal model

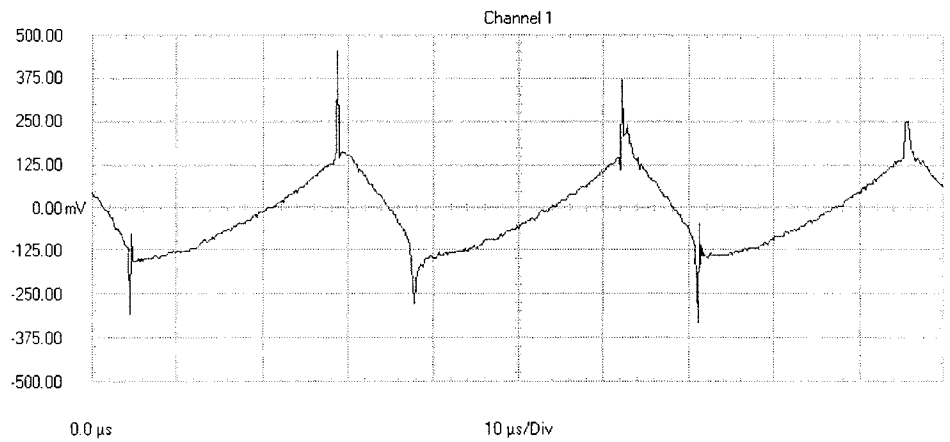

Figure 4.6: The experimental ripple at output voltage

Figure (4.6) shows the ripple at output voltage, for Buck2 experimental setup. The ripple is obtained in open-loop situation and at the operating point with $I_L = 2$A and $V_o = 20$V with buck converter system working in continuous-conduction mode.

It is to be noted that considerable differences exist between the ideal waveforms used in ripple analysis in Chapter 1 and the practically measured waveforms. The large signal model accurately predicts these waveforms.

4.3.1 Prediction of ripple from Fourier series model

In this section, Buck2 with parameters given in Appendix A is considered to illustrate the Fourier series method for computing the ripple. The open loop responses, with a fixed duty ratio of $d = 0.7177$, is calculated for different values of integer N in Fourier series model. For each value of N the matrices A, B and Q in (2.33) are constructed and the equation $AX = -QB$ is solved.

The size of this matrix A, when using Fourier series of order N, is $4N + 2$. After the Fourier coefficients are computed the time domain waveform is obtained using the coefficients and the values of $sin(k\omega_f t)$ and $cos(k\omega_f t)$ at fine steps of t where $\omega_f = \frac{2\pi}{T_s}$ and T_s is the switching period.

Figures 4.7 to 4.10 show the steady-state graphs for inductor current and capacitor voltage over one switching period.

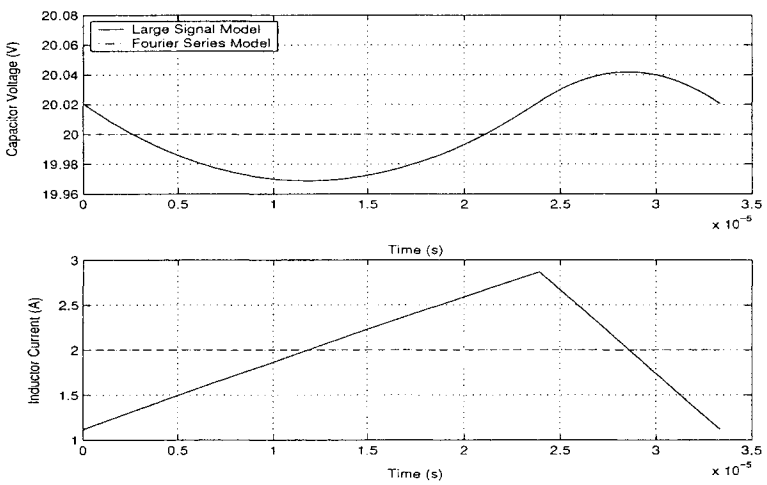

Figure 4.7: Open loop responses over one period with N=0

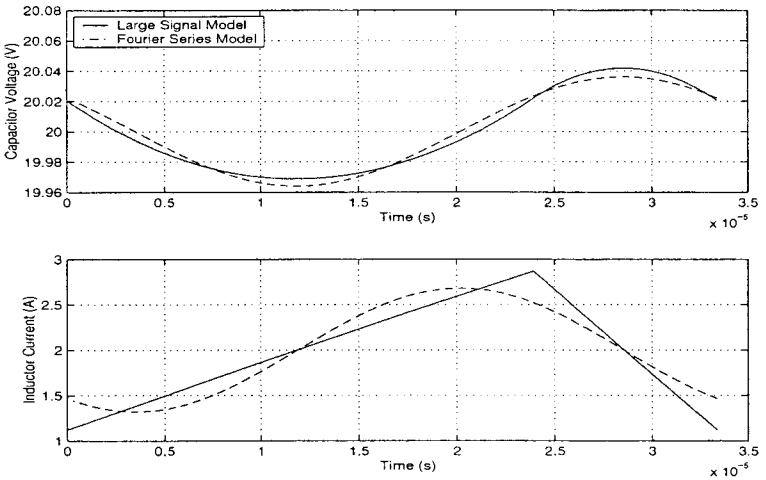

Figure 4.8: Open loop responses over one period with N=1

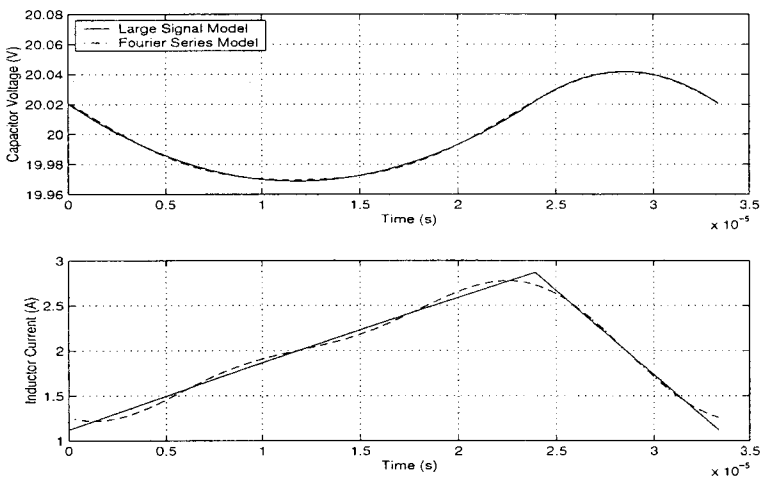

Figure 4.9: Open loop responses over one period with N=2

It can be seen that as the number of Fourier coefficients increases, the results from Fourier series model approaches the ones from the large signal model. Considering $N = 10$, which means the matrix A in the Fourier series model will be 42×42, the capacitor voltage will agree with the one obtained from the large signal model within 99.88% and the inductor current will agree with the one obtained from the large signal model within 97.67%. This example shows that Fourier series model deals with high order matrices that results in complex calculations as compared with the second order large signal model developed in this thesis.

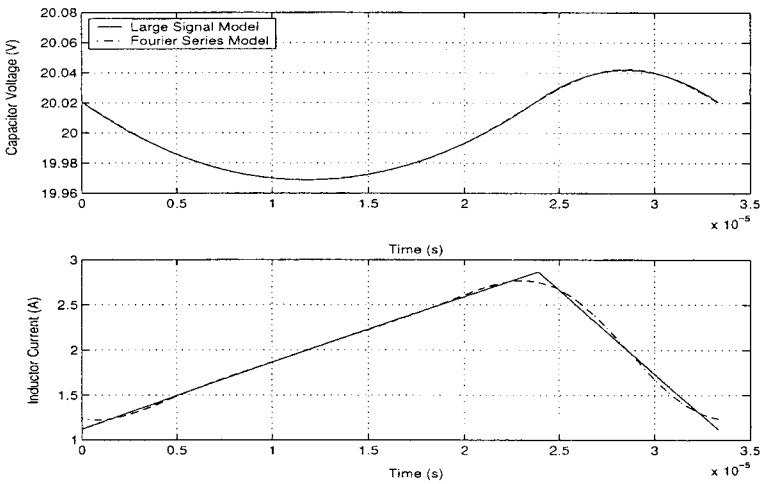

Figure 4.10: Open loop responses over one period with N=3

4.4 Conclusion

In this chapter, the performance of large signal model is studied. Large signal model can be used to predict amplitude and frequency of oscillations in a closed loop buck converter with a particular analog PI controller. Finding the amplitude of oscillation is not possible using the linear models.

Also large signal model is capable of predicting the steady-state behaviour of the buck converter. It gives the average of state variables at steady-state as well as the state variables waveform within a switching period. Fourier series model can also predict the steady-state behaviour but the large signal model is faster and less complicated for this purpose and the number of terms needed in the Fourier series is not an issue with it.

Chapter 5

Future work and conclusion

The results presented in this thesis so far were all obtained for constant values of load, inductance and input voltage V_d. However in a practical system, the load resistance changes, the inductance value varies based on the load current and temperature and the input voltage V_d fluctuates.

Some initial studies are accomplished by simulations using the large signal model to investigate the behaviour of buck converter when the load current, inductance and V_d are varying in continuous-conduction mode. The behaviour of buck converter is also studied for different values of switching frequency and different values of output voltage. The results are presented in this chapter and the potential use of these results in future work is mentioned.

5.1 Ripple

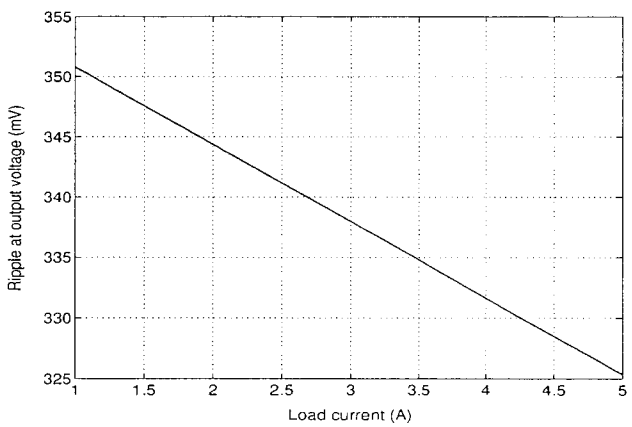

Figure 5.1: The peak-to-peak amplitude of ripple at the output of buck converter

The output voltage ripple for different values of load current is obtained from large

signal model. Figure 5.1 shows the peak-to-peak amplitude of ripple at the output voltage of Buck2 with parameters given in Appendix A.

As Figure shows the amplitude of ripple decreases with increasing load current. This behaviour, is also observed experimentally but can not be predicted from the ideal Equation (1.4). The parasitic parameters r_L and r_C, are not considered in (1.4) but they have an impact on ripple as the large signal model shows. Considering $r_L = 0$ and $r_C = 0$ the value of ripple calculated from large signal model is the same as ripple obtained from (1.4) for the ideal model (*i.e.* 75.6mV).

The output voltage ripple is also obtained for different inductor values from the large signal model. Figure 5.2 shows that the peak-to-peak value of ripple reduces when the value of the inductor is increased. From Equation (1.4), when L increases, f_c decreases and consequently the ripple decreases. So this trend can also be predicted by the ideal model even though the value of ripple calculated by (1.4) is not correct because r_C and r_L are not considered.

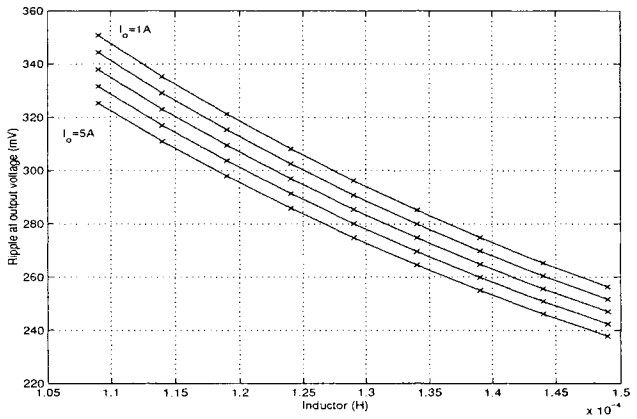

Figure 5.2: The variations of ripple with the inductor value

The value of ripple increases with increasing input voltage V_d which is also predicted by (1.4).

The variations of ripple as a function of switching frequency is shown in Figure 5.3 for Buck2 parameters with $V_o = 20$V. The value of ripple decreases significantly with increasing switching frequency. This can be also predicted from (1.4).

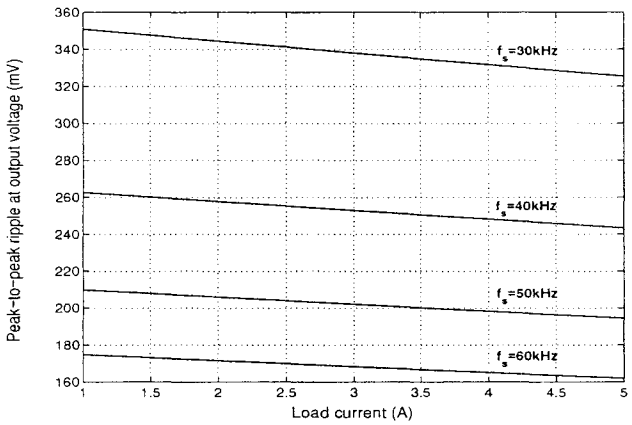

Figure 5.3: Ripple at the output of buck converter for different switching frequencies

5.2 Duty cycle

Figure 5.4 shows the relation between the duty cycle (which is proportional to control effort) for different values of steady-state current in continuous-conduction mode for Buck2.

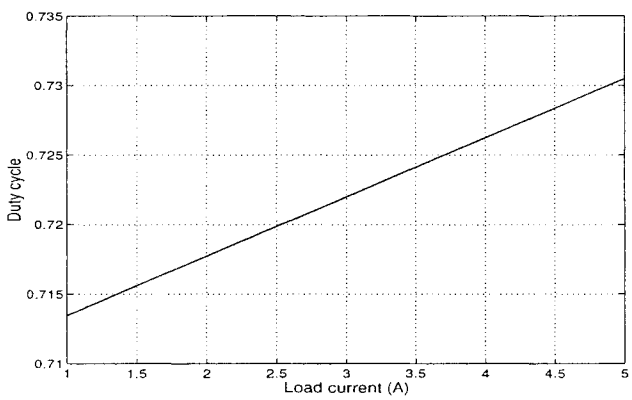

Figure 5.4: The variations of duty cycle with the load current

It can be seen that duty cycle is not constant for all values of load unlike the prediction of the ideal model of Chapter 1. The linear relations between duty cycles and load current for different values of output voltage is as follows,

for $V_o = 16\text{V}$, $D = 0.0043 \times i_o + 0.5674$
for $V_o = 20\text{V}$, $D = 0.0043 \times i_o + 0.7092$
for $V_o = 24\text{V}$, $D = 0.0043 \times i_o + 0.8511$.

It can be seen that the slope of the lines are equal for different values of output volt-

age. The following general equation can be used to model this,

$$D(i_o) = k \times i_o + \frac{V_o}{V_d} \tag{5.1}$$

where k is the proportionality constant and can be obtained for a specific buck converter.

5.3 Parallel buck converters

The basic requirement of parallel buck converters is that the individual converters share the load current equally and in a stable manner [19]. Different load-sharing schemes have been implemented to control each converter to maintain the desired voltage and equal current [20]. All these schemes require the measurement of current provided by each converter in some form or the other.

Normally, transducers are used to measure the inductor current but this is an expensive measurement either through loss of efficiency or direct cost. In this chapter it is seen that ripple at output voltage and duty cycle of buck converter vary with current. Hence the ripple and steady-state duty cycle could be used as an indirect way to estimate the load current and possibly the inductance of each converter. In order to use ripple as an estimation of load current, the buck converters in parallel could be working at different switching frequencies so the amplitude of ripple resulting from individual converters can be distinguished. Further investigation of this topic is future work emanating from this thesis.

5.4 Transient behaviour

The focus of this thesis, was mostly on the steady-state frequency-response behaviour of the buck converter. The large signal model is useful for predicting limit cycles as well as steady-state values of state variables and steady-state ripple. The large signal model can be used for computing the transient behaviour and for closed loop simulations and should be investigated in future work.

5.5 Conclusions

In this work, a ZOH equivalent discrete-time modeling approach to the buck converter is studied from the point of view of computing the large signal sinusoidal frequency-response of the buck converter. The study has been experimentally verified. The use of this large signal frequency-response in predicting limit cycles induced by output voltage feedback PI controllers for such converters is studied with experimental results. It is shown that the results so obtained provide a reasonably good approximation to the actual limit cycles obtained in an experimental converter under feedback.

Bibliography

[1] N.Mohan, T.M.Undeland & W.P.Robbins, "*Power Electronics: Converters, Applications, and Design*" John Wiley & Sons, 2nd Edition 1995.

[2] J.G.Kassakian, M.F.Schlecht and G.C.Verghese, *Principles of Power Electronics* Addison-Wesley Publishing Company, 1st edition 1991

[3] Edward P.Cunnigham, *Digital Filtering: An Introduction* Houghton Mifflin Company, 1992

[4] D.P. Atherton, "*Nonlinear Control Engineering*", Van Nostrand Reinhold, 1982.

[5] R.D. Middlebrook & S. Cuk, "A General Unified Approach to Modeling Switching Converter Power Stages", Proc. IEEE PESC-1976, pp. 18-34.

[6] S. Cuk & R.D. Middlebrook, "A General unified approach to modelling switching dc-to-dc converters in discontinuous conduction mode", IEEE PESC-1977, pp. 36-57.

[7] J. Van de Vegte, "*Feedback Control systems*", Prentice Hall, 3rd. Edition 1994.

[8] S.R. Sanders, J.M. Noworolski, X.Z. Liu & G.C. Verghese, "Generalized Avaraging Method for Power Conversion Circuits", IEEE. Trans. Power Electronics, Vol. 6, No. 2, pp. 251-259, 1991.

[9] V.A. Caliskan, G.C. Verghese & A.M. Stankovic, "Multifrequency Averaging of DC/DC Converters" IEEE Trans. Power Electronics vol. 14, No. 1, pp. 124-133, 1999.

[10] J.W. van der Woude, W.L. de Koning & Y. Fuad, "On the Periodic Behavior of PWM DC-DC Converters" IEEE Trans. Power Electronics vol. 17, No. 4, pp. 585-595, 2002.

[11] N. Femia, G. Spagnuolo & V. Tucci, "State-Space Models and Order Reduction in DC-DC Switching Converters in Discontinuous Modes", IEEE Trans. Power Electronics, Vol. 10, No. 6, pp. 640-650, 1995.

[12] A. Reatti & M.K. Kazimierczuk "Small-signal Model of PWM Converters for Discontinuous Conduction Mode and its Application for Boost Converter", IEEE Trans. Circuits and Systems-I, Vol. 50, No. 1, pp. 65-73, 2003.

[13] S.R. Sanders, "On Limit Cycles and the Describing Function Method in Periodically Switched Circuits", IEEE. Trans. Circuits and Systems-I, Vol. 40, No. 9, pp. 564-572, 1993.

[14] G. Franklin & J. D. Powell, "*Digital control of dynamic systems*", Addison-Wesley Pub. Co., 1980.

[15] E.A. El-Bidweihy & K. Al-Badwaihy, "Steady-State Analysis of Static Power Converters", IEEE Trans. on Ind. Appl. Vol. IA-18, No. 4, pp. 405-410, 1982.

[16] J.M. Burdio & A. Martinez, "A Unified Discrete-Time State-Space Model for Switching Converters", IEEE Trans. on Power Electronics, Vol. 10, No. 10, pp. 694-707, 1995.

[17] A. Ghosh & G. Ledwich, "Modeling and control of switch-mode DC-DC converters using state transition matrices", Int. Jou. of Electronics, Vol. 79, No. 1, pp. 113-127, 1995.

[18] D. Li & R. Tymerski, "Comparison of Simulation Algorithms for Accelerated Determination of Periodic Steady State of Switched Networks", IEEE Trans. on Ind. Electronics, Vol. 47, No. 6, pp. 1278-1285, 2000.

[19] David J. Perreault, Robert L. Selders, John G. Kassakian, "Frequency-Based Current-Sharing Techniques for Paralleled Power Converters" IEEE transactions on power electronics, Vol. 13, NO. 4, July 1998.

[20] Shiguo Luo, Zhihong Ye, Ray-Lee Lin and , Fred C. Lee. "A Classification and evaluation of paralleling methods for power supply modules" IEEE Annual Power Electronics Specialists Conference, v 2, p 901-908, 1999.

Appendix A

Frequency-response experimental setup

Experimental circuit to determine the frequency-response of buck converters are given in Figures A.1 and A.2.

A.1 Calculation of parameters

The buck converter parameters are calculated for a maximum output voltage of 20V at 5A with the following specifications, using ideal buck converter equations.

Input voltage $V_d = 28.2$V
Output voltage $V_o = 20$V
Maximum output current $I_{o,max} = 5$A
Maximum output ripple $\frac{\Delta V_o}{V_o} = 0.5\%$
Buck1 Switching Frequency $f_{s1} = 35$KHz
Buck2 Switching Frequency $f_{s2} = 30$KHz

The converters are designed to be operating in continuous-conduction mode. So the inequality $I_L > I_{LB}$ should be satisfied for them. Using the above mentioned value of $I_{o,max}$ (which is the same as $I_{L,max}$) and equation (1.3) the inequality can be written as,

$$5 > \frac{DT_s}{2L}(V_d - V_o)$$

that yields to the minimum value of the inductor L_{min},
$L > 19.4\mu$H for Buck1 with switching frequency $f_{s1} = 35$KHz
$L > 16.6\mu$H for Buck2 with switching frequency $f_{s2} = 30$KHz.

Having the maximum output ripple and from equation (1.4) the maximum cut off frequency f_c for the converters are obtained,
$f_c < 2066$Hz for Buck1 and $f_c < 1771$Hz for Buck2.

Using equation (1.5), $(LC)_{min}$ is calculated,
$LC > 5.9343 \times 10^{-}9$ for Buck1
$LC > 8.0772 \times 10^{-}9$ for Buck2.

Capacitor and Inductor values are chosen so that the inequality for $(LC)_{min}$ and L_{min} are satisfied. Table A.1 lists the chosen values for L and C and other parameters that are calculated for each buck converter circuit.

Table A.1: Characteristics of buck converters

Buck1	Buck2
$L_1 = 79\mu$H (MPP Core)	$L_2 = 109\mu$H (Air Core)
$r_{L_1}(dc) = 0.01\Omega$	$r_{L_2}(dc) = 0.12\Omega$
$C_1 = 98\mu$F	$C_2 = 98\mu$F
$V_d = 28.2$V	$V_d = 28.2$V
$V_o = 20$V	$V_o = 20$V
$f_s = 35$KHz	$f_s = 30$KHz
$\hat{V}_{st} = 10$V (0-10)	$\hat{V}_{st} = 10$V (0-10)
$I_{LB,max} = \frac{T_s V_d}{8L} \approx 1.2$A	$I_{LB,max} = \frac{T_s V_d}{8L} \approx 1$A
$f_c = \frac{1}{2\pi\sqrt{LC}} = 1.81$KHz	$f_c = \frac{1}{2\pi\sqrt{LC}} = 1.54$KHz
$\Delta V_{o_1} = 76.7$mV, 0.38%	$\Delta V_{o_2} = 75.6$mV, 0.38%

A.2 Load resistance

Initially, in the experimental setup, rheostats were used as load. But rheostats have high inductance that will affect the response of the buck converter, also because of the low tolerance of rheostats, the value of the resistor is unstable and very sensitive to heat and it will change throughout the experiment. So in order to get more reliable results from the experimental setup, rheostats were replaced by low-inductance resistive loads. For this experiment, two resistors of type MP9100, $5\Omega \pm 1\%$, were connected in series and used as a 10Ω constant load with additional resistances switched in parallel to it to step-increase and decrease load. MP9100 series are non-inductive resistors manufactured by CADDOCK Electronics, Inc. Their power rating is derated based upon the case temperature. So it is absolutely essential to calculate the power applied to the resistors and use proper heat-sink, based on thermal equation in MP9100 datasheet. For this experiment a small fan was used to keep the heat-sinks cool.

A.3 Inductor

The relationship between the magnetic field intensity H and the magnetic flux density B in a particular material is defined as permeability μ, ($\mu = \frac{B}{H}$). Permeability of magnetic materials are not constant but vary as a nonlinear function of B (hysteresis behavior). One of the determining factors in the value of an inductor is the permeability of the core material. If the core is made of linear magnetic material (*i.e.* with constant μ), the inductor value is constant, otherwise the inductor's value varies with current [2].

The inductor used for Buck1 is a Talema SD series with MPP (Molypermalloy Powder) as core material. The use of MPP cores provides a highly stable inductance with varying bias current. For Buck2 air core inductor, which offers great linearity on B-H graph, was chosen.

In the circuit model for inductors, the dc resistance of the winding r_L were considered in series with inductor.

A.4 Circuit hints

In this section some hints about the circuit conditions are mentioned. Considering these hints while setting up an experiment, could be useful.

A.4.1 Wiring

In experimental setup wires are chosen as short as possible because long wires in the circuit collect noise and increase resistive power losses. Especially in high power part of the circuit, *i.e.* buck converter, the capacitor, diode, inductor and load resistor are wired as close together as possible and thicker wires are used since they have smaller resistance.

A.4.2 Input Power Supply

Two 1000μF capacitors were paralleled to input power supply to reduce the ripple on V_d.

A.4.3 Ground isolation

The grounds of the low-power part of circuit (control circuit) and the high-power part (converter circuit) were isolated using an opto-isolator. The speed of opto-isolator chip should be more than the switching frequency of the circuit.

The power supply, providing voltage for isolated parts of the circuit should be plugged in to the power socket through a 'cheater plug', an isolator transformer or any other configurations that guarantees ground isolation.

Also since there are two different grounds in the circuit, differential probes should be used rather than normal probes for viewing signals on oscilloscope.

A.4.4 Bypassing

For using each IC in the circuit, the application information was followed and bypass capacitors were considered according to datasheets. Also a parallel combination of two capacitors (a 10μF electrolyte and 1nF ceramic) were connected to power supplies of low power part of the circuit to diminish noise and handle high current spikes from the power supplies. Each ground is connected to the main ground of the power supply through a separate route.

A.4.5 Power dissipation

Due to high switching rate, power will be dissipated on MOSFET. So to radiate the extra heat, a heat-sink is connected to MOSFET.

A.5 Data collection

Data was collected through RS232 serial interface of oscilloscope (Fluke PM3370B). The default acquisition length on oscilloscope is 512 data points for each trace. It is possible to increase the length of a trace from 512 points up to a maximum 8K points (without using extra memories) which is the setting for this experiment. 8K samples results in a trace length of 16 screens, or 160 divisions.

The sampling period depends on the main timebase of oscilloscope. For example if the main timebase is 10μs the total time that data is collected will be $10\mu\text{s}\times 160 = 1.6\text{ms}$ and the sampling period will be $\frac{1.6}{8000} = 0.2\mu\text{s}$.

A.5.1 FFT calculations

To measure the magnitude of frequency-response, the FFT of the collected input and output data are calculated. Considering the number of samples taken through oscilloscope is $N = 8000$, the sampling rate T for each frequency should be chosen so that the frequency under study is an integer multiple of the FFT window width $\frac{1}{NT}$, otherwise leakage in the desired frequency vector will lead to incorrect values.

Since input and output data cannot be collected at the same time, phase of frequency-response cannot be calculated using FFT. So input and output of circuit was connected to two channels of oscilloscope, in analog mode and the phase shift between them was calculated by,

$$\phi = \frac{T_d}{T} \times 360$$

where ϕ is phase difference in degrees, T is the period of the signals and T_d is the time delay between input and output signals.

Since this measurement is obtained from oscilloscope, the resolution of ϕ can be calculated as,

$$\phi_{res} = \frac{1}{50} \times 360 = 7.2\,\text{deg}$$

where 50 is the total number of divisions on oscilloscope screen.

A.6 Efficiency

Considering the discussion in previous sections, the power conversion efficiency of the buck converters can be improved significantly. Here the power efficiency of two buck converters are given. The efficiencies were calculated using in open-loop situation. In closed-loop, the circuit efficiency is slightly less than the given values and is dependent on controller gains.

Table A.2: Efficiency of buck converters

	V_i	I_i	V_o	I_o	Efficiency
Buck1	28.212V	1.449A	20.005V	1.976A	96.7%
Buck2	28.163V	1.497A	20.002V	1.978A	93.84%

It can be seen that the efficiency of Buck2 is less than Buck1 which is because of higher copper loss due to higher resistance of the inductor r_L in Buck2.

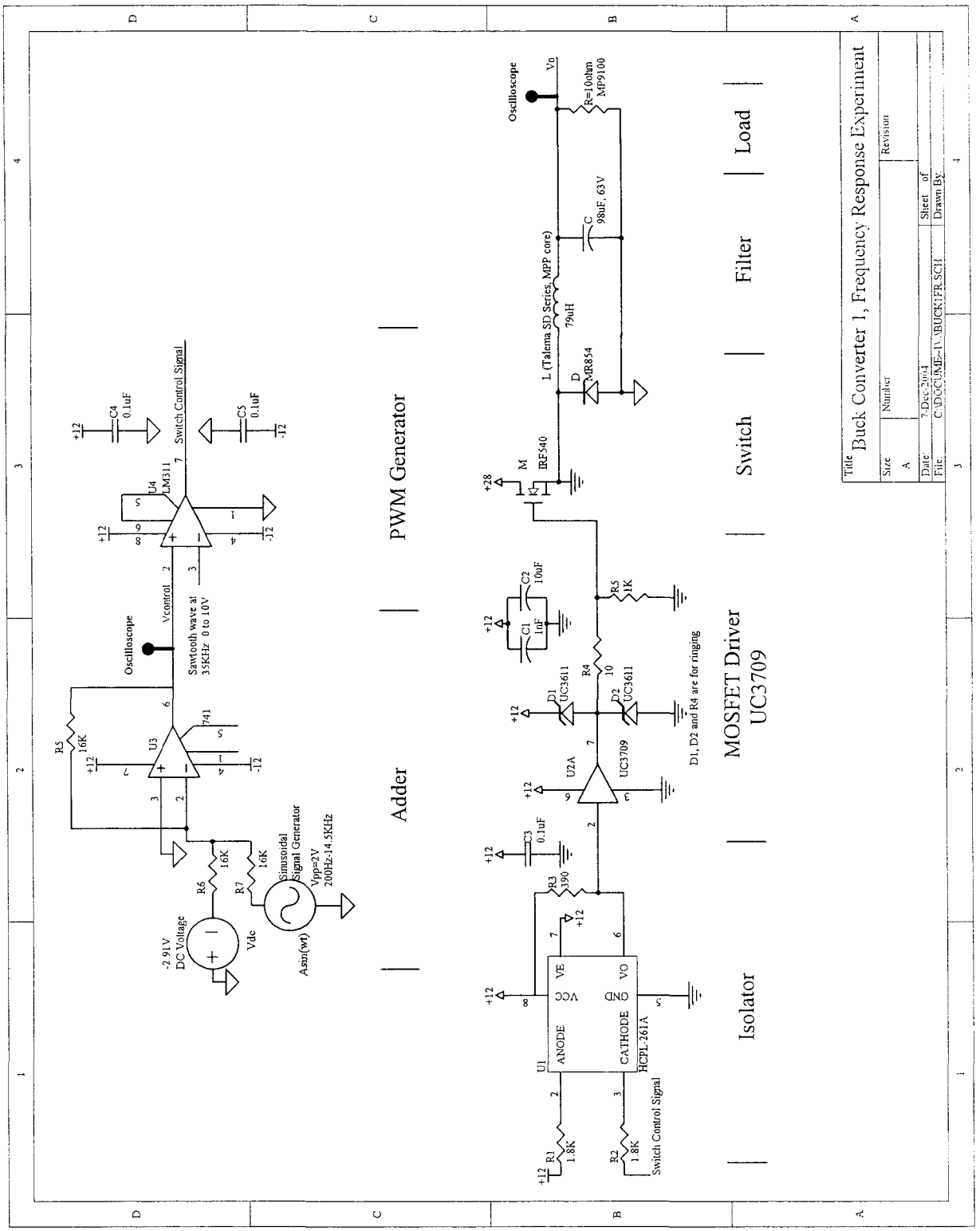

Figure A.1: Buck1 - experimental setup for frequency-response

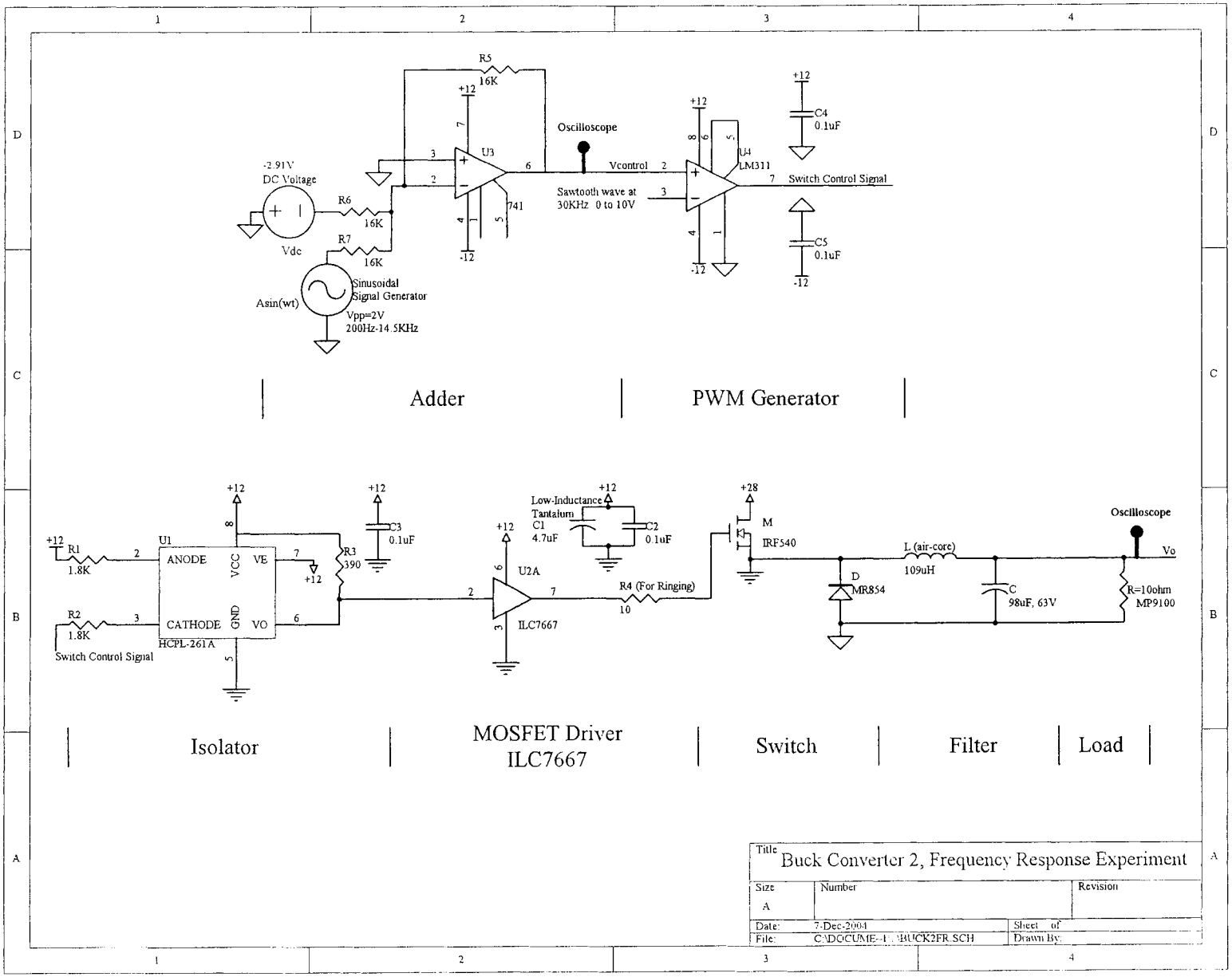

Figure A.2: Buck2 - experimental setup for frequency-response

Appendix B

Stability region experimental setup

Experimental circuit to determine the stability region of buck converters are given in Figures B.1 and B.2.

B.1 Subtracter circuit

The subtracter circuit used in the experimental setup is designed such that,

$$e = 2 \times 10V - V_o \tag{B.1}$$

where e is the error signal and $V_{ref} = 2 \times 10\text{V} = 20\text{V}$.

B.2 Controller circuit

A feedback control system is designed to maintain the output voltage at V_{ref}. The controller is a simple PI with the following form,

$$C(s) = K_P + \frac{K_I}{s}$$

with,

$$K_p = \frac{x1}{9.91K\Omega} \tag{B.2}$$

$$K_i = \frac{1}{0.096\mu F \times x2} \tag{B.3}$$

where $x1$ is the value of potentiometer $pot1$ in KΩ and $x2$ is the value of potentiometer $pot2$ in Ω which are adjusted to provide K_p and K_i gains respectively.

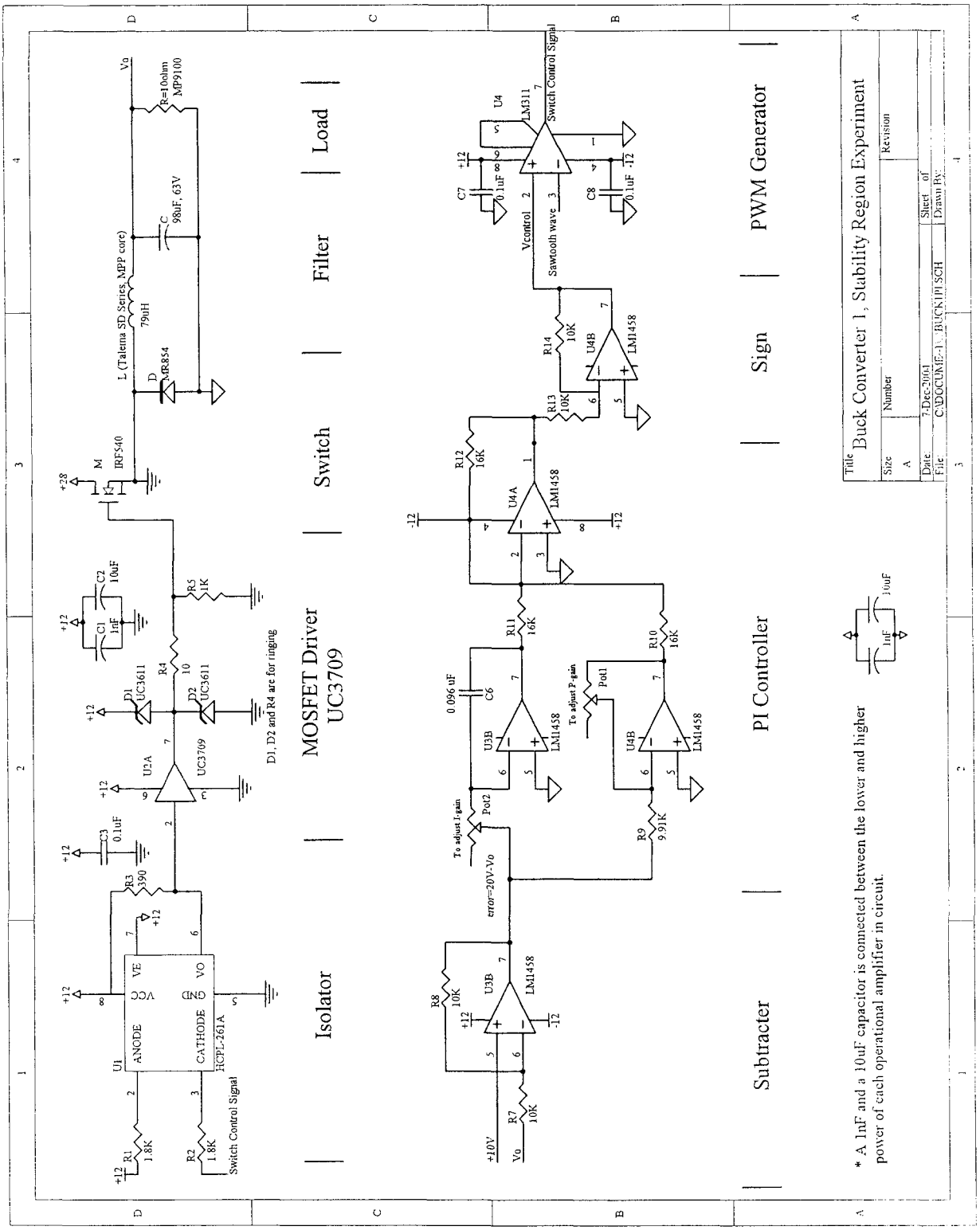

Figure B.1: Buck1 - experimental setup for stability region

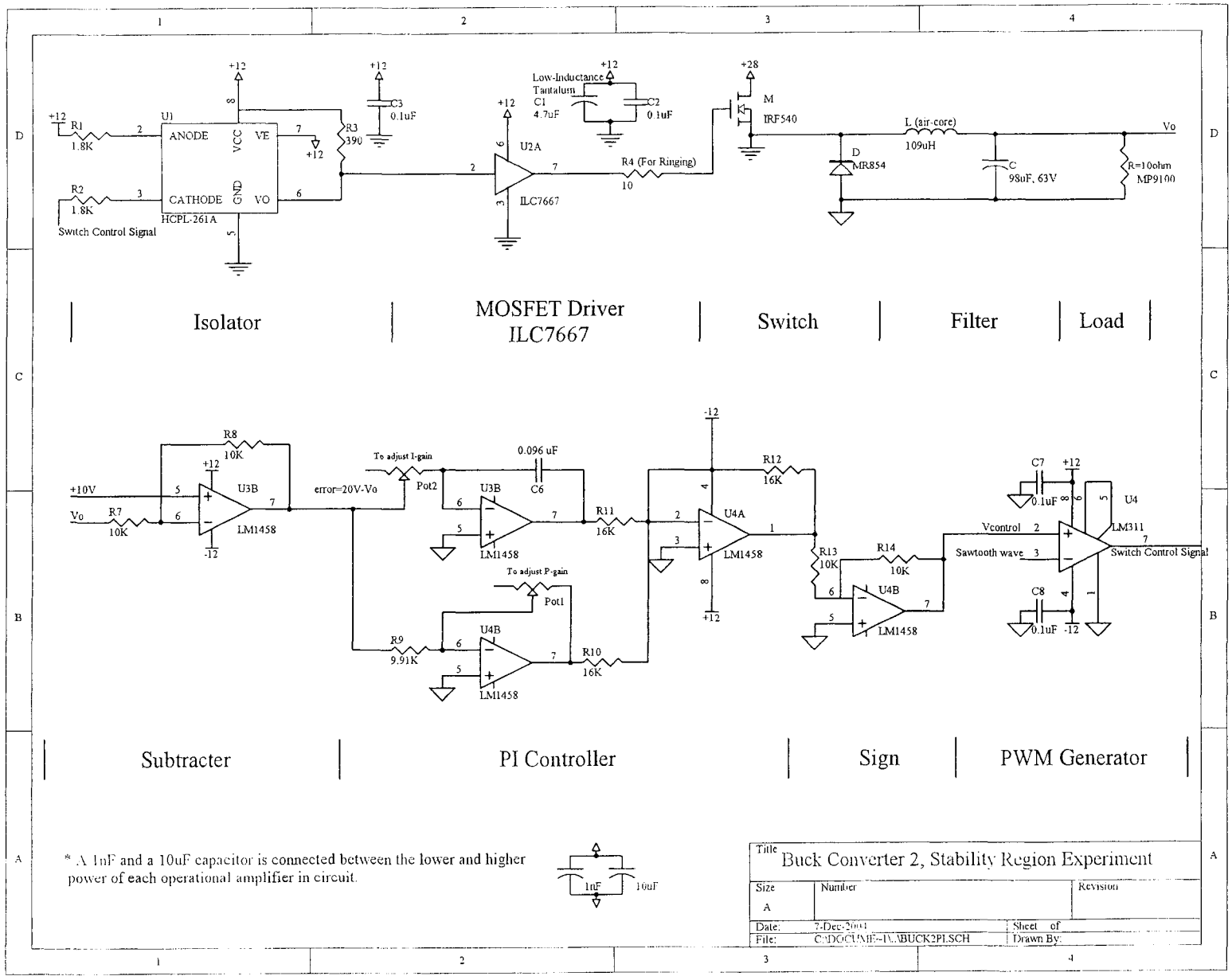

Figure B.2: Buck2 - experimental setup for stability region

Appendix C

Newton-Raphson method

In this appendix the formulation for the Newton-Raphson technique to determine the frequency-response is provided.

Considering $freq$ as the frequency at which the response is sought, and by choosing N and th as follows,

$$N = \frac{f_s}{freq} \tag{C.1}$$

$$th = \frac{2\pi}{N} \tag{C.2}$$

the state variables could be calculated for one period of input sine-wave. Figure C.1 shows the procedure.

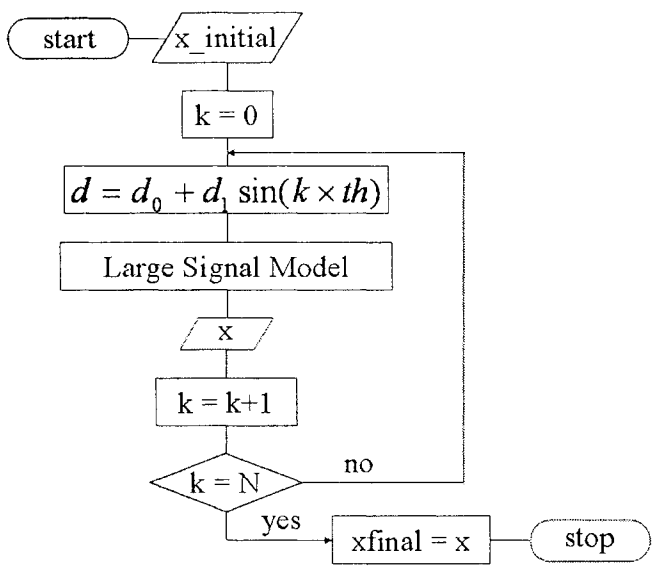

Figure C.1: Flowchart to calculate the output of large signal model for one period of sinusoidal input

Using Newton-Raphson iterations starting with some initial state variables, the state variables after one period of input sine-wave ($T = \frac{1}{freq}$) are calculated as follows,

- From the procedure explained in Figure C.1,
  - $xfinal$ is evaluated from $xinitial$
  - $xfinal_1$ is evaluated from $xinitial$ plus $perturbation$ in inductor current
  - $xfinal_2$ is evaluated form $xinitial$ plus $perturbation$ in capacitor voltage
- Jacobian matrix is made as, $J = \begin{pmatrix} \frac{xfinal_1 - xfinal}{perturbation} & \frac{xfinal_2 - xfinal}{perturbation} \end{pmatrix}$
- $error$ is found as, $xfinal - xinitial$
- δx is calculated as, $-(J - I)^{-1} \times error$
- $newx = xinitial + \delta x$

As shown in Figure C.2 the procedure explained above is continued in a loop till δx is less than a chosen $tolerance$ value (here 10^{-7}). The periodic steady-state vector is attained within a maximum of 5 iterations.

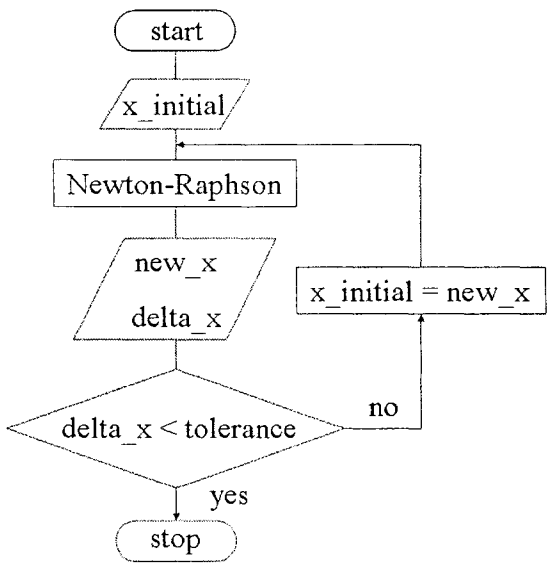

Figure C.2: Newton-Raphson technique

Comparing the obtained steady-state sinusoidal vector with the input sinusoid, the frequency-response magnitude and phase at the frequency $freq$ are calculated.

C.1 MATLAB functions

The following MATLAB functions are used for Newton-Raphson calculations.

```
function [J,new_x]=buck_freq_nraph(D0,D1,x_initial,freq)
fs=30e3;Rload=10;L=109e-6;C=98e-6;
rL=0.12;Vd=28.2;rC=0.2;
rsum=rC+Rload;
rparallel=rC*Rload/rsum;
Ts=1/fs;
output_C=[rparallel, Rload/rsum];
A=[-(rL + rparallel)/L  -(Rload/rsum)/L;(Rload/rsum)/C -1/(rsum*C)];
B=[Vd/L;0];
N=fs/freq;      % should be integer
% for example N=15 implies compute frequency response at fs/N
J=zeros(2,2);
th=2*pi/N;
x=x_initial;
for k=1:N
    D=D0+D1*sin(k*th);
    [F1,F2,F3,G1,flag,x1]=check_zero_crossing(A,B,x,Ts,D);
    x=x1;
end;
xfinal=x; % xfinal without perturbation
perturbation=1e-7;
% after computing J at different values of perturbation 1e-7
% seems to be best for this problem
x_perturb1=x_initial+[1;0]*perturbation;
x=x_perturb1;
for k=1:N
    D=D0+D1*sin(k*th);
    [F1,F2,F3,G1,flag,x1]=check_zero_crossing(A,B,x,Ts,D);
    x=x1;
end;
xfinal1=x; % xfinal with perturbation in inductor current
J(:,1)=(xfinal1-xfinal)/perturbation;
x_perturb2=x_initial+[0;1]*perturbation;
x=x_perturb2;
for k=1:N
    D=D0+D1*sin(k*th);
    [F1,F2,F3,G1,flag,x1]=check_zero_crossing(A,B,x,Ts,D);
    x=x1;
end;
xfinal2=x; % xfinal with perturbation in output voltage
J(:,2)=(xfinal2-xfinal)/perturbation;
x_error=xfinal-x_initial
delta_x=-inv(J-eye(2))*x_error
```

```
new_x=x_initial+delta_x
return;

function [F1,F2,F3,G1,flag,x1]=check_zero_crossing(A,B,x,Ts,D);
% flag=0 implies continuous conduction mode of buck converter operation
% flag=1 implies discontinuous conduction mode of buck converter operation.
% routine computes transition from state at one x to next x at Ts secs later.
[F1,G1]=discretize(A,B,D*Ts);
x=F1*x+G1;
[V,Lambda]=eig(A);
P=inv(V)*x;pa=P(1,1);pb=P(2,1);
V1=inv(V);
a=V1(1,1);b=V1(1,2);c=V1(2,1);d=V1(2,2);
phi=log(pb*b/(pa*d))/(Lambda(1,1)-Lambda(2,2));
phi=real(phi);
if (phi>=(1-D)*Ts)  % continuous-conducation mode
    flag=0;
    F3=eye(2);
    [F2,G2]=discretize(A,zeros(2,1),(1-D)*Ts);
    x1=F2*x;
else flag=1;      % if (phi<(1-D)*Ts)  % discontinuous-conduction mode
    [F2,G2]=discretize(A,zeros(2,1),phi);
    F3=eye(2);
    F3(2,2)=exp( ((1-D)*Ts-phi)*A(2,2) );
    x1=F2*x;x1(1,1)=0;
    x1=F3*x1;
end;
return;

function [f,g]=discretize(a,b,T)
% function computes discrete ZOH equivalent f,g of continous system matrices a,b
n=size(a);n=n(1,1);
[v,lam]=eig(a);vi=inv(v);f=v*diag(exp(diag(lam)*T))*vi;g=zeros(n);
for i=1:n,h=lam(i,i);if h~=0,g(i,i)=(exp(h*T)-1)/h;else g(i,i)=T;end;end;
g=v*g*vi*b;f=real(f);g=real(g);
return;
```